

1 **Global Climate Impacts of Greenland and Antarctic Meltwater: A**
2 **Comparative Study**

3 Qian Li^a, John Marshall^a, Craig D. Rye^{a,b}, Anastasia Romanou^b, David Rind^b, and Maxwell
4 Kelley^b

5 ^a *Department of Earth, Atmospheric, and Planetary Sciences, Massachusetts Institute of*
6 *Technology, Cambridge, MA, USA*

7 ^b *NASA Goddard Institute for Space Studies, New York, NY, USA*

8 *Corresponding author: Qian Li, qian_li@mit.edu*

9 ABSTRACT: Both Greenland and Antarctic ice sheets have been melting at an accelerating rate
10 over recent decades. Meltwater from Greenland might be expected to initiate a climate response
11 which is distinct, and perhaps different from, that associated with Antarctic meltwater. Which
12 one might elicit a greater climate response, and what mechanisms are involved? To explore
13 these questions, we apply “Climate Response Functions (CRFs)” to guide a series of meltwater
14 perturbation experiments using a fully coupled climate model. In both hemispheres, ice-sheet
15 meltwater drives atmospheric cooling, sea-ice expansion, and strengthened Hadley and Ferrel
16 cells. Greenland meltwater induces a weakening of the Atlantic Meridional Overturning Circulation
17 (AMOC) and a cooling of the subsurface ocean in the northern high-latitudes. Antarctic meltwater,
18 instead, induces a slowing of Antarctic Bottom Water production and a warming of the subsurface
19 ocean around Antarctica. For melt-rates up to 2000 Gt yr^{-1} , the climate response is rather linear.
20 However, as melt-rates increase to 5000 Gt yr^{-1} , the climate response becomes non-linear. Due
21 to a collapsed AMOC, the climate response is *super-linear* at high Greenland melt-rates. Instead,
22 the climate response is *sub-linear* at high Antarctic melt-rates due to the halting of the northward
23 expansion of Antarctic sea ice by warm surface waters. Finally, in the linear limit, we use CRFs
24 and linear convolution theory to make projections of important climate parameters in response to
25 meltwater scenarios, which suggest that Antarctic meltwater will become a major driver of climate
26 change, dominating that of Greenland meltwater, as the current century proceeds.

27 SIGNIFICANCE STATEMENT: Melting of Greenland and Antarctic ice sheets is one of the
28 most uncertain potential contributors to future climate change. In this study, we address the
29 comparative role of Greenland and Antarctic meltwater in the climate system and explore the
30 differing mechanisms at work in each hemisphere. We find that the climate response is linear
31 for low melt-rates but becomes non-linear for high melt-rates. As the century proceeds, we
32 speculate that Antarctic meltwater will increasingly dominate that of Greenland meltwater, leading
33 to atmospheric cooling, Antarctic sea-ice expansion, and contraction and warming of Antarctic
34 Bottom Water. Greenland meltwater will instead affect smaller changes local to the North Atlantic.

35 **1. Introduction**

36 Greenland and Antarctic ice sheets represent the largest land store of freshwater over the globe
37 which, should they completely melt and flow into the ocean, could contribute a total of 7.5 m and
38 58 m to global mean sea level, respectively (Morlighem et al. 2017; Fretwell et al. 2013). Recent
39 observations have shown that these ice sheets are melting at an accelerating rate (Paolo et al. 2015;
40 Rignot et al. 2019; Mouginit et al. 2019; Shepherd et al. 2018, 2020; King et al. 2020). Between
41 1992–2011 and 2012–2017, the rate of ice mass loss has risen from roughly 100 Gt yr⁻¹ to 200 Gt
42 yr⁻¹ in Greenland (Shepherd et al. 2020) and from 75 Gt yr⁻¹ to roughly 200 Gt yr⁻¹ in Antarctica
43 (Shepherd et al. 2018). Since the 1990s, their combined contribution to global mean sea level
44 has been 18 mm, of which 10 mm came from Greenland (Shepherd et al. 2020) and 8 mm from
45 Antarctica (Shepherd et al. 2018). Greenland ice mass loss is ice-sheet-wide owing to rapidly
46 increasing surface melting and ice dynamical imbalances (King et al. 2020). Antarctic ice mass
47 loss is largely due to ice-shelf basal melt and iceberg calving in roughly equal magnitude along the
48 periphery, primarily in the Amundsen-Bellinghshausen Sea sectors (West Antarctica), Wilkes Land
49 (East Antarctica), and the West and Northeast Peninsula (Rignot et al. 2019). Twenty-first-century
50 simulations of Greenland and Antarctic ice sheets forced with time-evolving ocean and climate
51 fields derived from a high-emission scenario, suggest the projected melt-rates exceeding 500 Gt
52 yr⁻¹ and 5000 Gt yr⁻¹ by 2100, respectively, leading to a total sea level rise in excess of 250 mm
53 with meltwater feedback (Golledge et al. 2019).

54 Ice-sheet meltwater contributes not only to sea level but also initiates climate change through its
55 effect, for example, on sea-ice extent and the ocean's overturning circulation. One might expect the

56 impacts of Greenland meltwater to be different from that of Antarctic meltwater, because they act in
57 different hemispheres and perturb different parts of the climate system. For example, it is thought
58 that Antarctic meltwater spreading to the proximal ocean initiates surface cooling and freshening
59 trends across the Southern Ocean (Bronse laer et al. 2018; Rye et al. 2020). Enhanced basal melt
60 of Antarctic ice shelves (Rignot et al. 2013; Depoorter et al. 2013; Adusumilli et al. 2020) can
61 cause significant sea-ice expansion by suppressing convective mixing and its associated vertical
62 heat exchange (Hellmer 2004; Bintanja et al. 2013). Meltwater discharge along the Antarctic
63 continental shelf tends to weaken Antarctic Bottom Water (AABW) and the lower overturning cell
64 (Silvano et al. 2018; Lago and England 2019; Li et al. 2022). Meltwater discharge from Greenland,
65 meanwhile, can reduce deep ocean ventilation via a slowdown in the formation rate of North
66 Atlantic Deep Water (NADW) originating in the Nordic (Greenland-Iceland-Norwegian (GIN))
67 Seas (Böning et al. 2016), and a weakening of the Atlantic Meridional Overturning Circulation
68 (AMOC) (Rahmstorf et al. 2015; Bakker et al. 2016). Antarctic meltwater can also affect the
69 AMOC, but the sense of the change remains controversial. Stouffer et al. (2007) found that the
70 AMOC remains unchanged or slightly weakened due to Antarctic meltwater spreading across the
71 sea surface in the North Atlantic. However, Weaver et al. (2003) suggested that Antarctic meltwater
72 rather intensifies the strength of the AMOC and NADW formation via a change in the potential
73 density relationship between water masses. But then, these effects are damped by Greenland
74 meltwater. Such competing climate impacts become even more intriguing when it is realized that
75 increasing differences between Greenland and Antarctic melt-rates are expected, with the Antarctic
76 source likely to increasingly dominate over Greenland in the coming decades (Golledge et al. 2019).

77 Addressing these issues is important, not least to explore the uncertainties in climate projections
78 undertaken for the latest Coupled Model Intercomparison Project Phase 6 (CMIP6; Eyring et al.
79 2016). These projections do not account for dynamic ice sheet melt, thus lacking a key component of
80 the cryosphere system. That said, many recent climate model simulations have applied meltwater
81 scenarios either around Greenland (Hu et al. 2011; Bakker et al. 2016; Putrasahan et al. 2019;
82 Orihuela-Pinto et al. 2022) or Antarctica (Bakker and Prange 2018; Bronse laer et al. 2018; Rye
83 et al. 2020; Mackie et al. 2020; Beadling et al. 2022). Taken together, these studies suggest that
84 Greenland meltwater is projected to weaken the AMOC significantly by 2100 in both intermediate
85 and high emission scenarios (Hu et al. 2011; Bakker et al. 2016), although intermodel differences

86 are still evident (Bakker et al. 2016). By 2100 under a high-emission scenario, Antarctic meltwater
87 is projected to drive a series of notable changes, inducing a decrease in global-mean surface air
88 temperature, an increase in sea-ice area, a northward shift of Intertropical Convergence Zone, and
89 Antarctic coastal warming associated with a marked on-shelf intrusion of warm Circumpolar Deep
90 Water (Bronse laer et al. 2018).

91 The primary motivation of the current study is (i) to identify the key mechanisms which control
92 the response of the climate system to Greenland and Antarctic meltwater, and (ii) to quantify the
93 efficacy of Greenland vs. Antarctic meltwater in instigating global climate change. We will contrast
94 the impacts of Greenland and Antarctic meltwater through a series of perturbation experiments
95 using a fully coupled climate model. We undertake three sets of experiments in which the same
96 amount of meltwater is released along the land-ocean boundary of Greenland and Antarctica, both
97 separately and together. We carry out the experiments in the framework provided by “Climate
98 Response Functions (CRFs)” and linear convolution theory (Hasselmann et al. 1993). Here, the
99 CRFs represent the response of climate parameters to a step-change in meltwater forcing, and the
100 response to a linear-ramp forcing can be inferred by convolution to the extent that the response is
101 linear. As successfully applied in many previous studies (Gregory et al. 2015; Marshall et al. 2014,
102 2017a; Rye et al. 2020; Lembo et al. 2020), this framework enables us to compare the relative
103 contributions of different hemispheric meltwater sources on the global climate.

104 Our paper is organized as follows. In Section 2, the coupled model and experimental design are
105 described. Sections 3 and 4 respectively contrast the global impacts and mechanisms in response
106 to Greenland and Antarctic meltwater. Section 5 discusses the response functions for meltwater
107 forcing and their application to make future projections of climatically important parameters, such
108 as surface air temperature, sea-ice extent and strength of the AMOC. Finally, in Section 6, we
109 discuss and conclude.

110 **2. The coupled model and experimental design**

111 *a. The global climate model*

112 We employ the E2.1-G version of the National Aeronautics and Space Administration (NASA)
113 Goddard Institute for Space Studies (GISS) Earth system model, denoted GISS-E2.1-G (Kelley et al.
114 2020; Miller et al. 2021; Nazarenko et al. 2022). GISS-E2.1-G is a coupled climate model designed

115 to simulate the earth system comprising representations of the atmosphere, ocean, land and sea ice.
116 The atmospheric model component has a horizontal resolution of $2^\circ \times 2.5^\circ$ latitude by longitude
117 and 40 vertical pressure layers. The vertical coordinate transitions from a terrain-following sigma
118 tropospheric representation below 150 hPa to constant-pressure stratospheric layers above this
119 level, all the way up to the model top at 0.1 hPa. In this E2.1-G version, a new option facilitates a
120 smooth transition centered at 100 hPa with a half-width of approximately 30 hPa. The dynamical
121 core, atmospheric mixing, convection and boundary layer models are described in more detail in
122 (Kelley et al. 2020).

123 The ocean model component of E2.1-G version has a horizontal resolution of $1^\circ \times 1.25^\circ$ latitude
124 by longitude and 40 vertical layers. It is mass-conserving with a free surface and natural surface
125 boundary conditions for heat and freshwater fluxes (Russell et al. 1995). The model employs a
126 version of the boundary layer *K*-profile parameterization (KPP) of vertical mixing (Large et al.
127 1994) and the Gent and McWilliams (GM) parameterization (Gent et al. 1995) with variable
128 coefficients (Visbeck et al. 1997) for eddy tracer fluxes induced by mesoscale baroclinic turbulence.
129 In E2.1-G, the parameterization of mesoscale eddy transport is updated with a moderate-complexity
130 3-D mesoscale diffusivity inspired by the studies presented in Marshall et al. (2017b). The vertical
131 diapycnal diffusivity incorporates a new tidal mixing scheme via a dissipation distribution given by
132 Jayne (2009), which improves the representation of the AMOC. Additional developments include
133 the use of higher-order advection schemes (Prather 1986), finer upper-ocean layering and more
134 realistic representation of flow through straits that affect property distributions in marginal seas
135 (Kelley et al. 2020).

136 The sea-ice model component consists of two mass layers within each of which are two thermal
137 layers. Sea ice salinity and tracer values are calculated on the atmospheric grid in the horizontal
138 and the mass layers in the vertical. Sea-ice dynamics is based on a formulation of the standard
139 viscous-plastic rheology (Zhang and Rothrock 2000). Sea-ice thermodynamics includes a “Brine
140 Pocket” parameterization (Bitz and Lipscomb 1999) that allows salt to play a more active role in
141 the specific heat and melt-rates of the sea ice.

142 The ice sheet model has no representation of ice flow dynamics, and its iceberg calving rates
143 are determined (Tournadre et al. 2016), for each ice sheet, as those balancing its accumulation
144 of mass from precipitation minus evaporation and surface melt (Schmidt et al. 2014). Iceberg

145 calving fluxes into the adjacent oceans are adjusted over 10 years time-lagged relative to the ice
146 sheet accumulation, which is operative to represent ice sheet dynamics timescales in the model
147 background state.

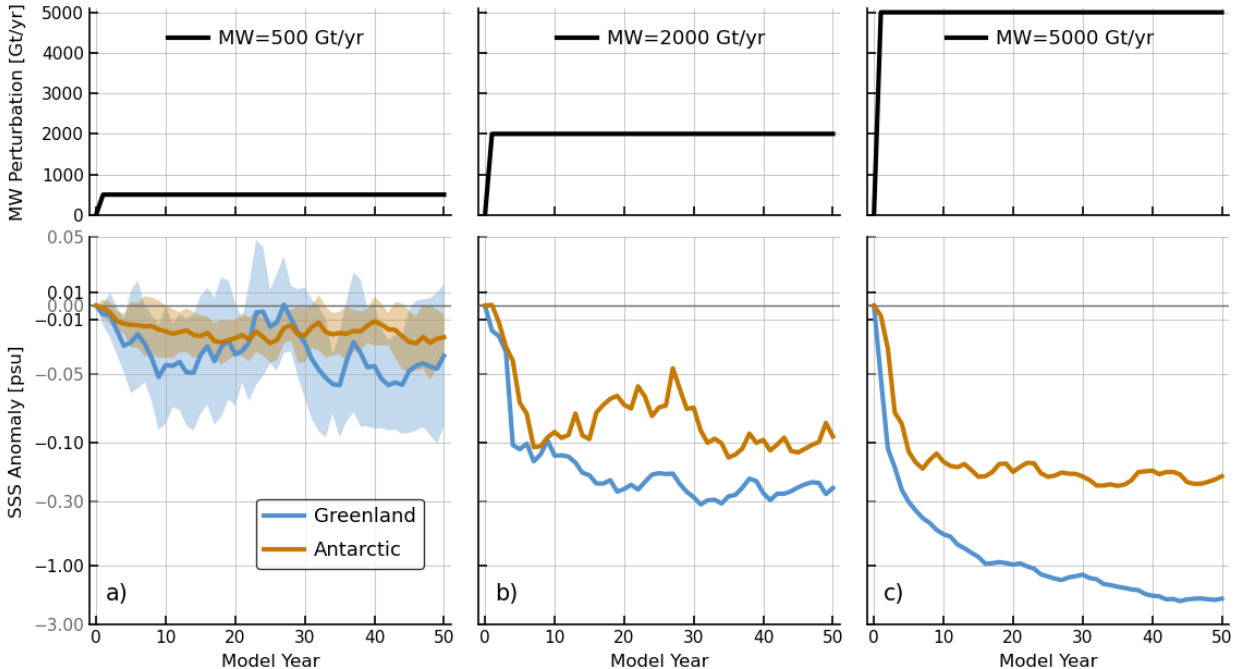
148 The GISS-E2.1-G model has a pleasingly realistic climatology in a long pre-industrial control
149 simulation, particularly in its representation of the Southern Hemisphere atmosphere, ocean and
150 sea-ice distributions — see Kelley et al. (2020) and Miller et al. (2021). Our model simulates a
151 notably realistic mixed layer depth distribution in the Southern Ocean (Supplementary Figs. S1a
152 and S1c), suggesting that convection forms in plausible locations along the Antarctic continental
153 shelf. However, the modeled mixed layers are too deep in the North Atlantic (Supplementary Figs.
154 S1b and S1d), suggesting that there is excessive mixing in the deep ocean (Lerner et al. 2021). The
155 modeled seasonal cycle of Antarctic sea ice also agrees rather well with observations (Kelley et al.
156 2020). The wintertime Arctic sea-ice extent, however, exceeds that seen in observations, perhaps
157 due to excess heat loss to the atmosphere (Kelley et al. 2020).

158 *b. Experimental design*

159 Here we consider three scenarios in which meltwater is released along the land-ocean boundary
160 of Greenland or Antarctica, both separately and together, as summarised in Table 1. Then, a
161 step-function forcing is applied in which the melt-rate is instantaneously stepped up from zero to
162 500 Gt yr^{-1} ($\sim 0.016 \text{ Sv}$) in one experiment, 2000 Gt yr^{-1} ($\sim 0.06 \text{ Sv}$) in another and finally 5000 Gt
163 yr^{-1} ($\sim 0.16 \text{ Sv}$) to yield three experiments for each scenario, or nine in all (see the top panels of
164 Fig. 1). These amplitudes are inspired by the current and projected melt-rates ranging from several
165 hundred up to 5000 Gt yr^{-1} by 2100, as noted in the Introduction. We follow the algorithm and
166 procedure described in Rye et al. (2020). The meltwater fluxes and associated cooling anomalies,
167 stemming from extraction of the latent heat required to melt ice, are distributed over the upper 200
168 meters, making use of the mask of the iceberg array as shown in Fig. 2. Note that we impose
169 the meltwater perturbation in the near-surface layers, neglecting spatial complexity due to the
170 contribution of basal melt at depth. In addition, we distribute the meltwater perturbation evenly
171 along the continental margins, in an attempt to represent the lateral dispersion of freshwater from
172 the coast. The model's background ocean circulation advects the implied sea surface salinity (SSS)

TABLE 1. Experimental design for nine meltwater perturbation experiments.

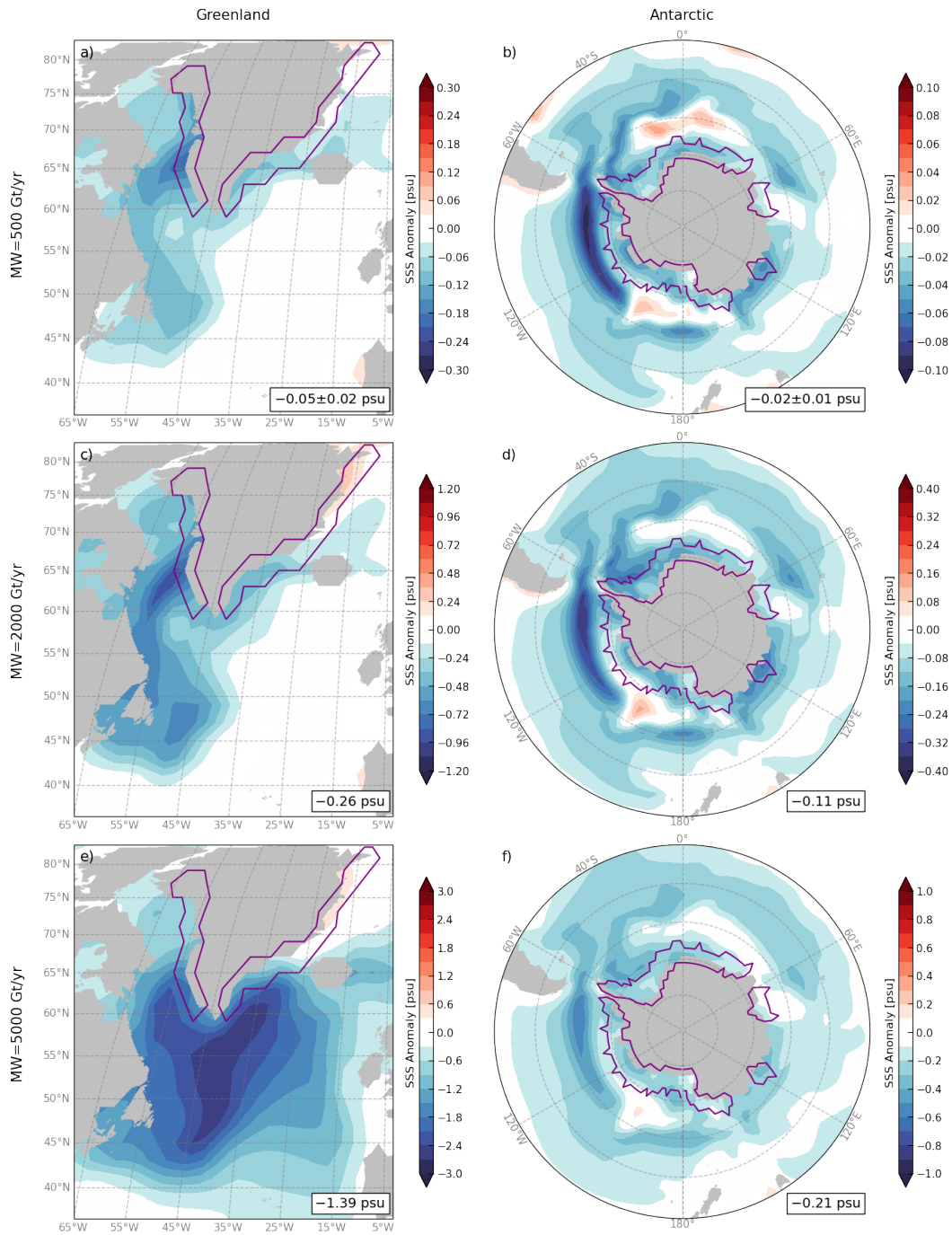
| Meltwater (MW) Forcing Schemes | | 500 Gt/yr (~0.016 Sv) | 2000 Gt/yr (~0.06 Sv) | 5000 Gt/yr (~0.16 Sv) |
|------------------------------------|--------------------------|---|--------------------------|--------------------------|
| Scenarios (Ensemble Members) | Greenland MW | 10 | 1 | 1 |
| | Antarctic MW | 10 | 1 | 1 |
| | Greenland & Antarctic MW | 10 | 1 | 1 |
| Primary & Extended Periods | | 50 & 100 years | 50 & 100 years | 50 & 100 years |
| Distribution | | Distributed evenly along the continental margins in the upper 200 m | | |



175 FIG. 1. Time series of step-change meltwater forcings of a) 500 Gt yr⁻¹, b) 2000 Gt yr⁻¹ and c) 5000 Gt yr⁻¹ (top
 176 panels) and SSS anomalies (psu; bottom panels) averaged over the North Atlantic sector (45°–80°N, 5°–65°W)
 177 in the Greenland scenario (blue) and the Southern Ocean sector (50°–90°S, 0°–360°E) in the Antarctic scenario
 178 (orange). In the bottom panel of a), shading represents one standard deviation model spread for ten ensemble
 179 members, and the line represents the ensemble-mean in the 500 Gt yr⁻¹ case. Note that in the bottom panels, the
 180 y-axis SSS scale is non-linear.

173 anomalies away from the coast along freshwater pathways, as an approximate alternative to the
 174 advection of icebergs away from the margin.

187 In order to contrast the global impacts and mechanisms of meltwater alone over the next several
 188 decades, all nine idealized meltwater perturbation experiments are initiated from a long pre-
 189 industrial control of 5,650 years and then run on in parallel for 50 years. The experiments in which



181 FIG. 2. SSS anomalies (psu) averaged over 50 years for a, c, e) the North Atlantic sector (45°–80°N, 5°–65°W)
 182 in the Greenland scenario and b, d, f) the Southern Ocean sector (50°–90°S, 0°–360°E) in the Antarctic scenario
 183 with meltwater forcings of 500 Gt yr⁻¹, 2000 Gt yr⁻¹ and 5000 Gt yr⁻¹, respectively. Purple contours indicate
 184 the Greenland and Antarctic areas where meltwater is fluxed into the ocean. Spatially-averaged SSS anomalies
 185 (with one standard deviation for ten ensemble members in the 500 Gt yr⁻¹ case) are indicated in the boxes in the
 186 bottom right of each panel.

190 a relatively small perturbation of 500 Gt yr^{-1} is carried out employ ten ensemble members. This,
191 through averaging, enables us to dampen the effect of internal variability. Experiments, which
192 assume much larger perturbations of 2000 Gt yr^{-1} and 5000 Gt yr^{-1} , have a more robust response
193 and so need only employ one ensemble member. For the analyses of CRFs and convolutions,
194 all the simulations are extended out to 150 years. This enables us to explore longer timescales
195 and particularly temporal variability of the AMOC. The control experiments with pre-industrial
196 forcings carried out alongside these perturbations do not employ any meltwater forcing. The
197 difference between concurrent periods of perturbation and control is analyzed to minimize the
198 influence of model drift on our results.

199 Note that in our figures the range of the colormap scales linearly with the magnitude of three
200 meltwater forcings, enabling us to examine the linearity of atmospheric and ocean responses to
201 meltwater forcing.

202 *c. Freshwater pathways*

203 We first check the behavior of our solutions by examining the temporal evolution and spatial
204 distribution of SSS anomalies obtained in response to meltwater scenarios. The SSS adjustment
205 overall reaches a new quasi-steady state in about 10 years, apart from that with the Greenland
206 melt-rate of 5000 Gt yr^{-1} , as shown in the time series of SSS (Supplementary Fig. 2) and SSS
207 anomaly (see the bottom panels of Fig. 1). Due to the difference in land-ocean distribution and
208 ocean circulation, surface freshening is confined to a small geographic area around Greenland,
209 but extends over a larger area across the Southern Ocean. The freshwater pathways around
210 Greenland simulated from our model show a plausible pattern in accord with Gillard et al. (2016).
211 Specifically, freshwater release from west Greenland accumulates in Baffin Bay and then flows down
212 the Labrador shelf; freshwater from east Greenland largely flows into the interior of the Labrador
213 Sea, where deep convection occurs. Indeed, with Greenland meltwater, surface freshening spreads
214 primarily along the Labrador Current in the 500 Gt yr^{-1} and 2000 Gt yr^{-1} cases (Figs. 2a and 2c),
215 but extends more widely across the subpolar North Atlantic in the 5000 Gt yr^{-1} case (Fig. 2e). As
216 a result, SSS decreases by -0.05 psu and -0.26 psu over the North Atlantic sector (45° – 80°N , 5° –
217 65°W) respectively in the 500 Gt yr^{-1} and 2000 Gt yr^{-1} cases, close to linear scaling. However, SSS
218 dramatically decreases by -1.39 psu in the 5000 Gt yr^{-1} case. In contrast, with Antarctic meltwater

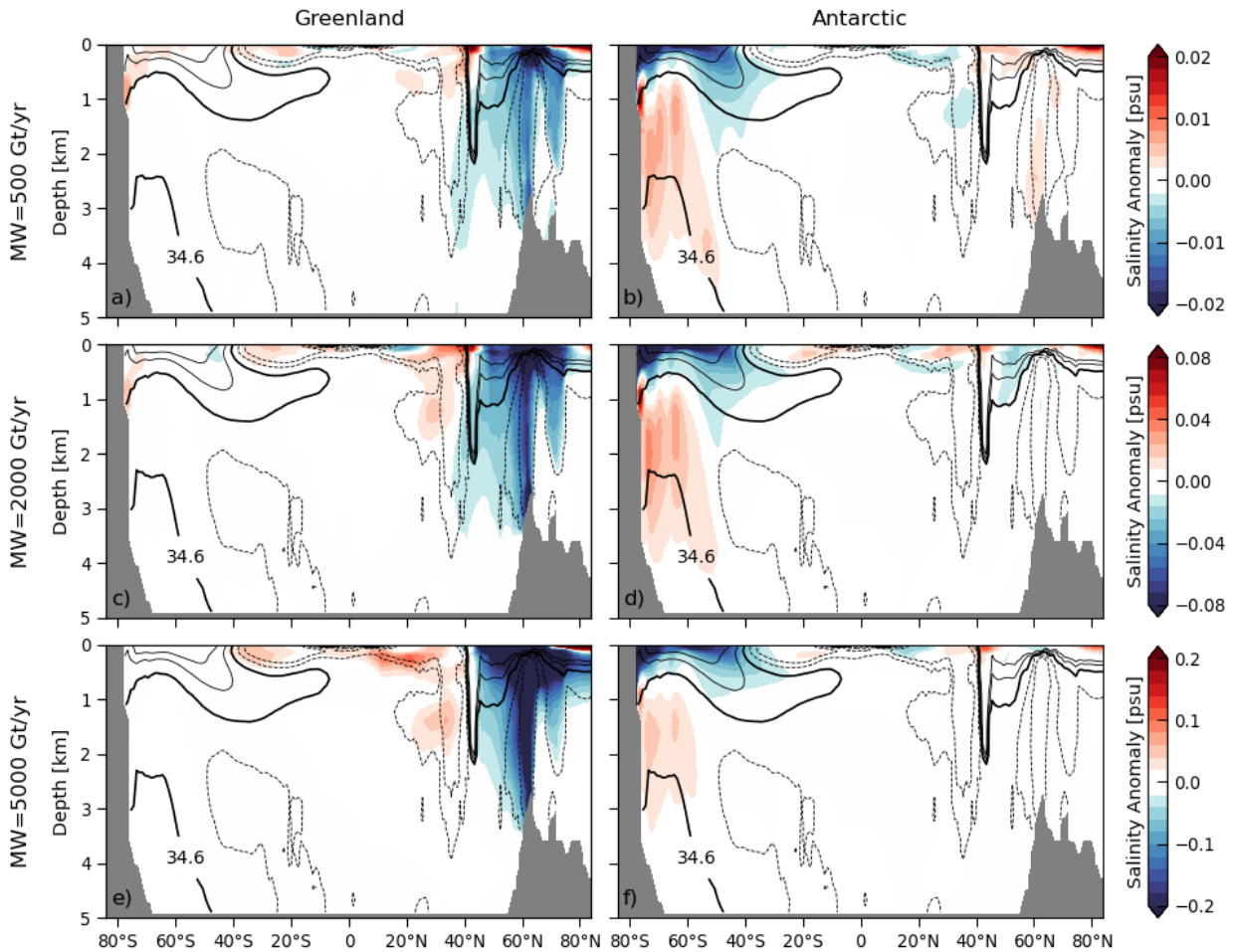
219 spreading across the Southern Ocean, SSS anomaly is diluted and scales roughly linearly with the
220 magnitude of three meltwater forcings: we observe the decreases of -0.02 psu, -0.11 psu and -0.21
221 psu over the Southern Ocean sector (50°–90°S, 0°–360°E), respectively (Figs. 2b, 2d and 2f). The
222 linearity of the response, or otherwise, will be discussed in more detail in subsequent sections.

223 In the ocean interior, freshwater pathways are distinct between the Greenland and Antarctic
224 scenarios. With Greenland meltwater, anomalous freshening penetrates to the deep ocean in
225 the northern high-latitudes (Figs. 3a, 3c and 3e). With Antarctic meltwater, however, anomalous
226 freshening largely extends down to 1-km depth in the southern mid-latitudes, following the pathways
227 of formation and subduction of mode and intermediate waters. The surface ocean freshens around
228 Antarctica, but the deep ocean becomes saltier (Figs. 3b, 3d and 3f).

235 **3. Differing Global impacts of Greenland and Antarctic meltwater**

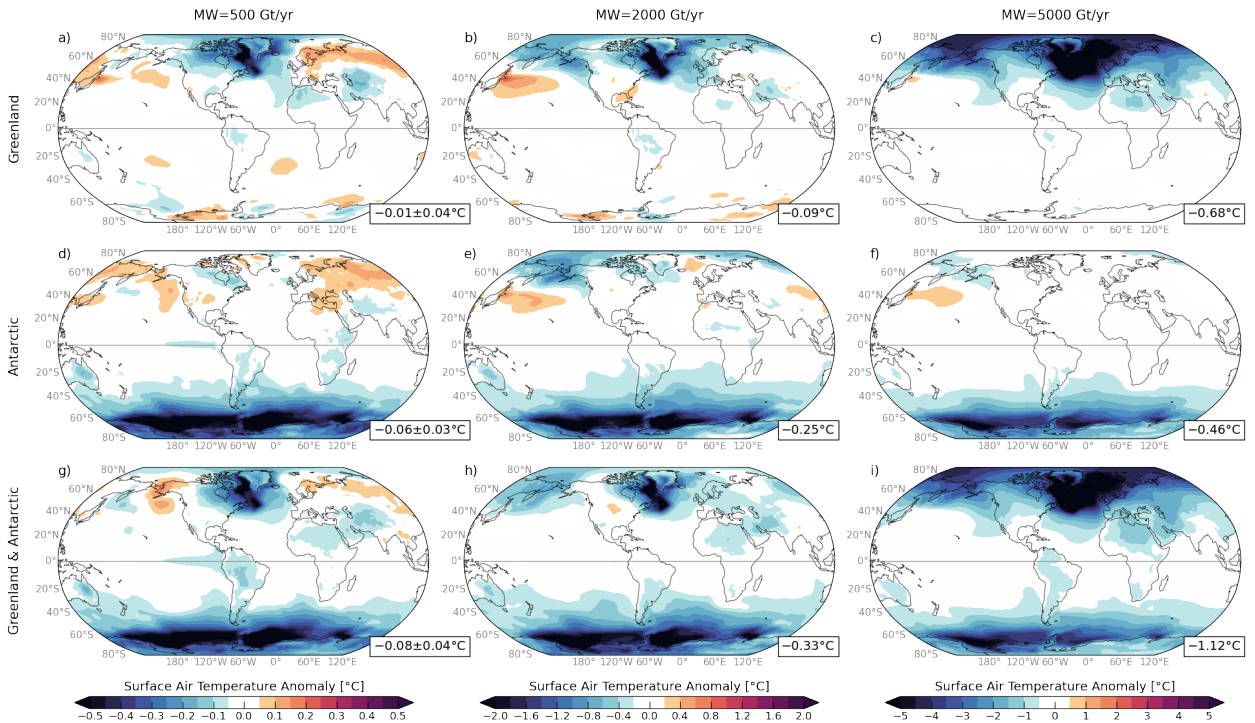
236 *a. Global surface response*

237 To contrast the large-scale impacts of Greenland and Antarctic meltwater, surface air temperature
238 anomalies from all nine perturbation experiments are presented in Fig. 4. Overall, surface air
239 temperature experiences a substantial cooling, particularly local to the source of meltwater input.
240 With the relatively small Greenland melt-rates of 500 Gt yr⁻¹ and 2000 Gt yr⁻¹, anomalous surface
241 cooling is apparent in the subpolar North Atlantic (Figs. 4a and 4b). As melt-rates increase to
242 5000 Gt yr⁻¹, anomalous surface cooling occurs across the entire Northern Hemisphere (Fig. 4c).
243 As a result, the global-mean surface air temperature decreases by -0.01°C, -0.09°C and -0.68°C
244 in the 500 Gt yr⁻¹, 2000 Gt yr⁻¹ and 5000 Gt yr⁻¹ cases, respectively (Figs. 4a-c). Note that
245 the response is *greater* than what would be expected if the response was linear (super-linear) in
246 the 5000 Gt yr⁻¹ case (Fig. 4c). By comparison, with all three Antarctic melt-rates, anomalous
247 surface cooling covers a wide area across the Southern Hemisphere. The global-mean surface air
248 temperature decreases by -0.06°C, -0.25°C, and -0.46°C in the 500 Gt yr⁻¹, 2000 Gt yr⁻¹ and 5000
249 Gt yr⁻¹ cases, respectively (Figs. 4d-f). Note that the response, however, is *less* than what would
250 be expected if the response was linear (sub-linear) in the 5000 Gt yr⁻¹ case (Fig. 4f). In sum,
251 surface air temperature anomaly scales linearly with the forcing amplitude moving from 500 Gt
252 yr⁻¹ to 2000 Gt yr⁻¹ but, as mentioned, this linear relationship breaks down in the 5000 Gt yr⁻¹
253 case. Furthermore, surface air temperature anomaly in the simultaneous Greenland and Antarctic



229 FIG. 3. Vertical cross-sections of the zonal-mean ocean salinity anomalies (psu; color) averaged over 50
 230 years in the a, c, e) Greenland and b, d, f) Antarctic scenarios with meltwater forcings of 500 Gt yr^{-1} , 2000 Gt
 231 yr^{-1} and 5000 Gt yr^{-1} , respectively. Contours represent the climatological-mean ocean salinity from the control
 232 runs with an interval of 0.2 psu . The bold line is the 34.6 psu contour, marking the low-salinity tongue of
 233 Antarctic Intermediate Water extending to depth in the mid-latitudes of the Southern Ocean. Thin dashed and
 234 solid contours denote values above and below 34.6 psu (thick solid contour), respectively.

254 scenario is close to the sum of that in separate Greenland and Antarctic scenarios (Figs. 4g-i).
 255 The global-scale cooling is dominated by Antarctic meltwater in the 500 Gt yr^{-1} and 2000 Gt yr^{-1}
 256 cases, but it is surpassed by Greenland meltwater in the 5000 Gt yr^{-1} case.



257 FIG. 4. Surface air temperature anomalies ($^{\circ}\text{C}$) averaged over 50 years in the a, b, c) Greenland, d, e, f)
 258 Antarctic and g, h, i) simultaneous Greenland and Antarctic scenarios with meltwater forcings of 500 Gt yr^{-1} ,
 259 2000 Gt yr^{-1} and 5000 Gt yr^{-1} , respectively. Globally-averaged surface air temperature anomalies (with one
 260 standard deviation for ten ensemble members in the 500 Gt yr^{-1} case) are indicated in the boxes in the bottom
 261 right of each panel.

262 *b. Atmospheric and ocean response*

263 The zonal-mean atmospheric and ocean temperature anomalies are further examined (Fig. 5). In
 264 the atmosphere, meltwater drives anomalous cooling over the full vertical extent of the troposphere.
 265 With melt-rates of 500 Gt yr^{-1} and 2000 Gt yr^{-1} , the Antarctic-meltwater-driven cooling in the
 266 Southern Hemisphere is stronger and extends more equatorward to the tropics than the Greenland-
 267 meltwater-driven cooling in the Northern Hemisphere (Figs. 5a, 5b, 5d and 5e, top panels). As
 268 Greenland melt-rates increase to 5000 Gt yr^{-1} , atmospheric cooling intensifies dramatically and
 269 becomes super-linear in the Northern Hemisphere (Fig. 5c, top panel). Instead, as Antarctic
 270 melt-rates increase to 5000 Gt yr^{-1} , atmospheric cooling in the Southern Hemisphere becomes
 271 sub-linear (Fig. 5f, top panel).

272 In the ocean, the temperature shows opposite responses to meltwater forcing in the two hemi-
273 spheres: we observe the Greenland-meltwater-driven cooling north of 45°N and the Antarctic-
274 meltwater-driven cooling south of 45°S. As Greenland melt-rates increase from 500 Gt yr⁻¹ through
275 2000 Gt yr⁻¹ to 5000 Gt yr⁻¹, ocean cooling amplifies super-linearly (Figs. 5a-c, bottom panels).
276 In contrast, ocean warming responds in a sub-linear way to three Antarctic melt-rates (Figs. 5d-f,
277 bottom panels).

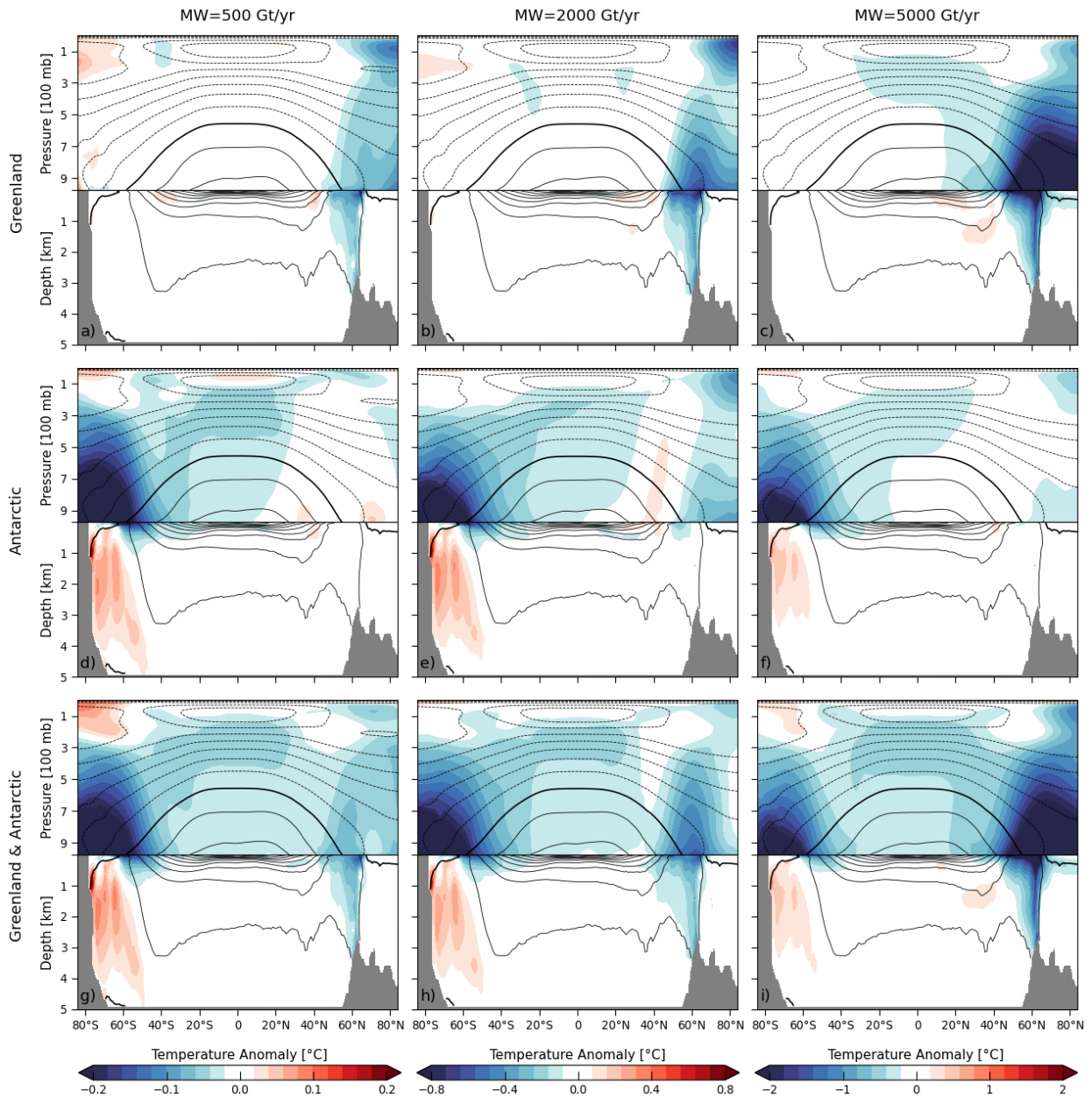
284 Meltwater also drives large-scale changes in atmospheric and ocean meridional overturning
285 circulations (MOCs), shown in Fig. 6. Here we quantify the atmospheric MOC in sverdrups (Sv),
286 where 1 Sv=10⁹ kg s⁻¹ (see e.g., Czaja and Marshall 2006). This definition is used because it enables
287 us to use the same unit for both the atmosphere and ocean overturning streamfunctions. In addition,
288 the ocean MOC is the total streamfunction that includes the eddy component. The climatological-
289 mean atmospheric MOC contains three hemispherically symmetric cells: the Hadley cell, Ferrel
290 cell and Polar cell. With meltwater from either Greenland or Antarctica, the atmospheric MOC
291 anomaly shows a stronger Ferrel cell and a greater latitudinal extent for the equatorial Hadley Cell
292 in each hemisphere (Figs. 6a-f, top panels). By comparison, these changes are more evident with
293 the relatively large melt-rates.

294 Furthermore, the climatological-mean ocean MOC includes two global-scale thermohaline over-
295 turning cells: an upper cell linked to the AMOC and a lower cell driven by AABW formation and
296 export (Marshall and Speer 2012). With enhanced stratification due to meltwater injection, the
297 upper and lower cells both experience a significant slowdown. As Greenland melt-rates increase
298 from 500 Gt yr⁻¹ through 2000 Gt yr⁻¹ to 5000 Gt yr⁻¹, the upper cell declines super-linearly (Figs.
299 6a-c, bottom panels). However, the lower cell is weakened in a sub-linear way to three Antarctic
300 melt-rates (Figs. 6d-f, bottom panels).

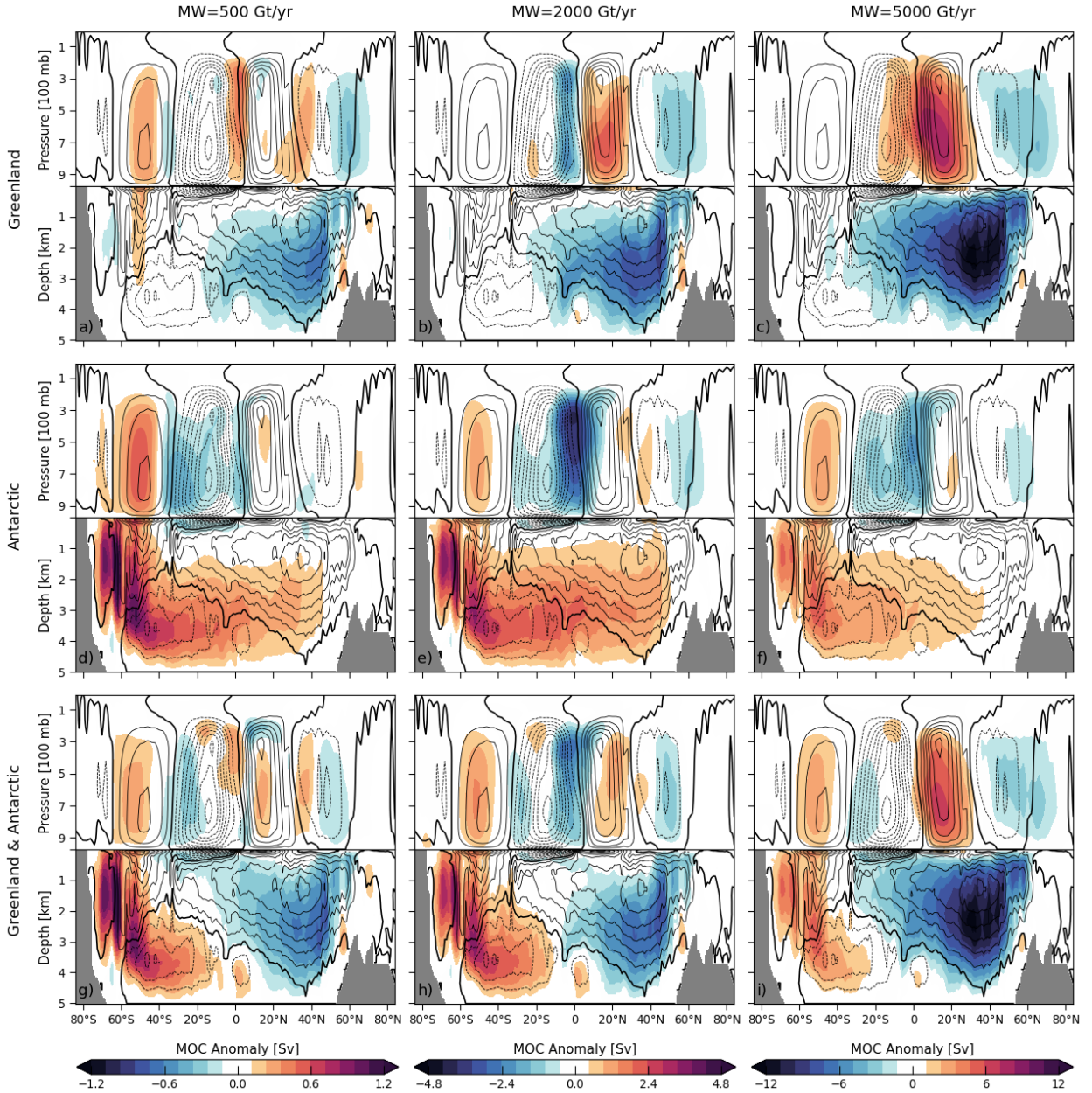
307 **4. Contrast of mechanisms controlling the climate response to Greenland and Antarctic** 308 **meltwater**

309 *a. Sea ice response*

310 The global impacts of Greenland and Antarctic meltwater are reflections of common but also
311 distinct mechanisms at work in each hemisphere. With Greenland meltwater, anomalous surface
312 cooling in the North Atlantic is likely due to diminished northward transport of heat caused by



278 FIG. 5. Vertical cross-sections of the zonal-mean atmospheric and ocean temperature anomalies ($^{\circ}\text{C}$; color)
 279 averaged over 50 years in the a, b, c) Greenland, d, e, f) Antarctic and g, h, i) simultaneous Greenland and
 280 Antarctic scenarios with meltwater forcings of 500 Gt yr^{-1} , 2000 Gt yr^{-1} and 5000 Gt yr^{-1} , respectively. Contours
 281 represent the climatological-mean atmospheric and ocean temperature from the control runs with intervals of
 282 10°C and 3°C , respectively. Dashed, solid and bold contours denote the negative, positive and zero values,
 283 respectively.

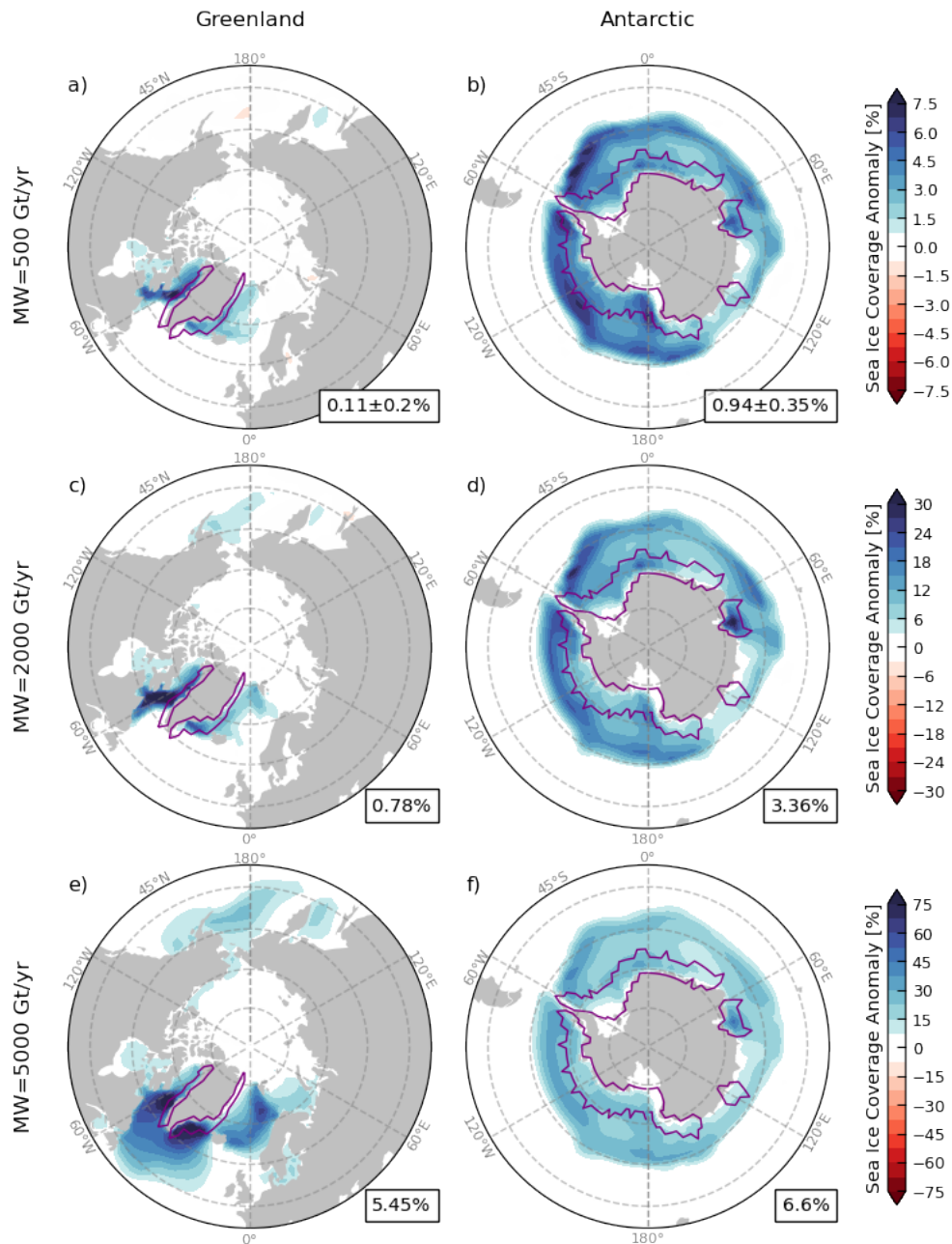


301 FIG. 6. Vertical cross-sections of the zonal-mean atmospheric and ocean MOC anomalies (Sv; color) averaged
 302 over 50 years in the a, b, c) Greenland, d, e, f) Antarctic and g, h, i) simultaneous Greenland and Antarctic
 303 scenarios with meltwater forcings of 500 Gt yr^{-1} , 2000 Gt yr^{-1} and 5000 Gt yr^{-1} , respectively. Contours represent
 304 the climatological-mean atmospheric and ocean MOC from the control runs with intervals of 12 Sv and 4 Sv,
 305 respectively. Dashed, solid and bold contours denote the negative (anticlockwise), positive (clockwise) and zero
 306 values, respectively. The ocean MOC is represented as the total streamfunction that includes the eddy component.

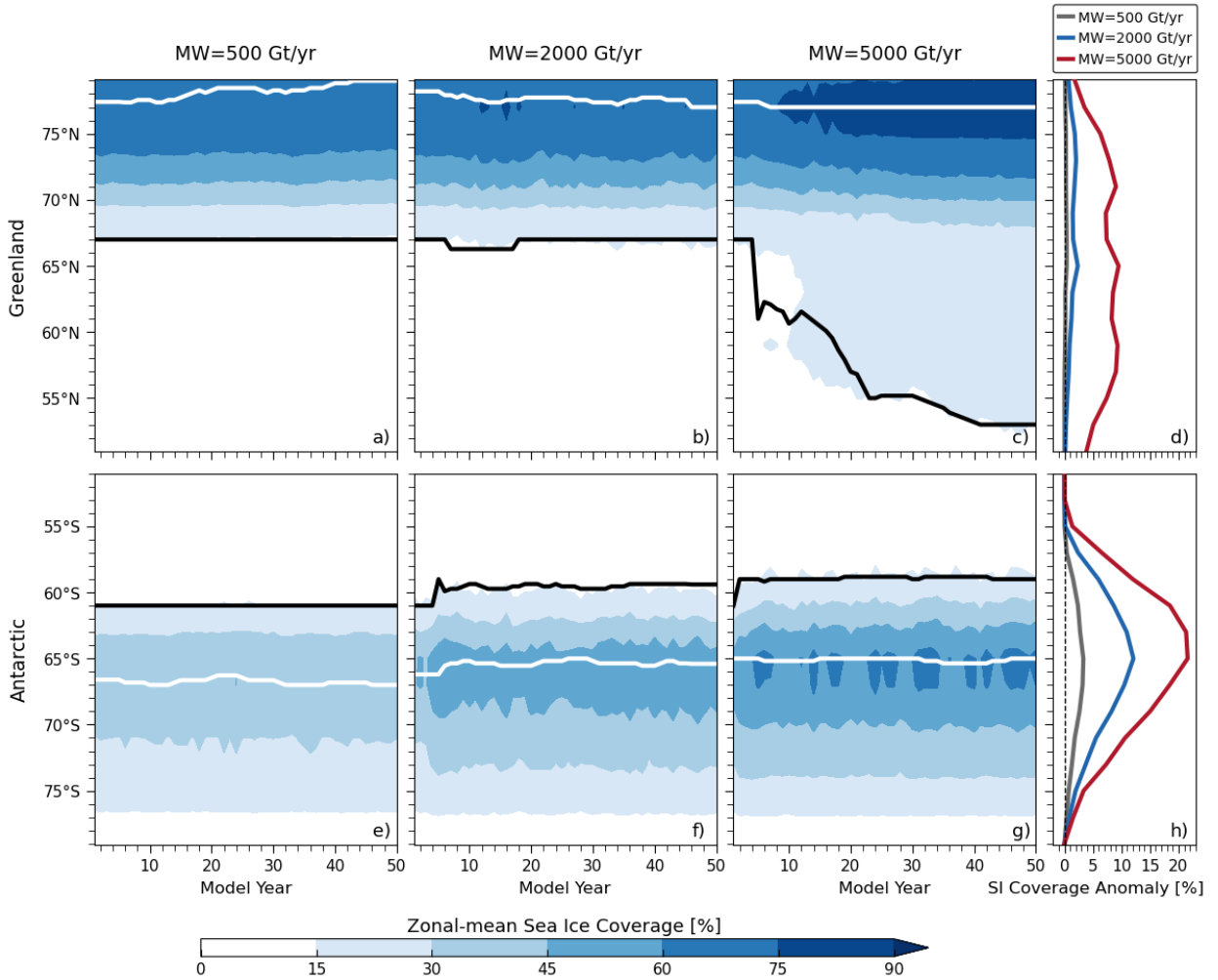
313 the AMOC slowdown (Buckley and Marshall 2016; Orihuela-Pinto et al. 2022). With Antarctic
314 meltwater, instead, a lessening of vertical heat exchange due to enhanced upper-ocean stratification
315 suppressing convection, leads to anomalous surface cooling across the Southern Ocean (Richardson
316 et al. 2005; Zhang 2007; Bintanja et al. 2013; Pauling et al. 2016). In addition, sea ice grows for
317 two possible reasons: (i) an elevated freezing point of seawater due to enhanced surface freshening
318 and cooling, and (ii) an increased percentage of incoming solar radiation reflected back to space
319 via positive ice-albedo feedback. Indeed, an increase in sea-ice coverage is evident with meltwater
320 from either Greenland or Antarctica (Fig. 7).

321 With Antarctic meltwater, sea ice expands over a wide geographic area in longitude (Figs. 7b,
322 7d and 7f), causing and coinciding with hemispheric surface cooling anomalies observed around
323 Antarctica (Figs. 4d-f). In a recent study, Rye et al. (2022) highlighted that the widely distributed
324 sea ice can reduce the water vapor transfer from the southern high-latitudes to the tropics, which
325 can further drive a global-scale atmospheric cooling via negative water-vapor feedback. This
326 Antarctic-meltwater-driven atmospheric cooling can compensate for greenhouse-gas-driven global
327 warming by potentially 10 to 30% in the mid-century. In contrast, with Greenland meltwater, sea
328 ice covers only a small area due to a different land-ocean distribution. For instance, sea ice grows
329 mostly along the Labrador Sea in the 500 Gt yr⁻¹ and 2000 Gt yr⁻¹ cases (Figs. 7a and 7c), but also
330 expands past over the Denmark Strait and across the Irminger Sea in the 5000 Gt yr⁻¹ case (Fig.
331 7e). Note that within a 50-year time frame, sea-ice coverage is more geographically confined than
332 that of hemispheric surface cooling (Figs. 4a-c). This indicates that other mechanisms for surface
333 cooling in the Northern Hemisphere are likely at work in the Greenland scenario.

341 The temporal evolution of sea-ice coverage is suggestive of different non-linear responses to
342 Greenland and Antarctic meltwater. With Greenland meltwater, the sea-ice edge, referred to as the
343 latitude of 15 percent sea-ice concentration, extends northward up to a latitude of 67°N in the 500
344 Gt yr⁻¹ and 2000 Gt yr⁻¹ cases (Figs. 8a and 8b), but extends dramatically beyond 53°N in the 5000
345 Gt yr⁻¹ case (Figs. 8c and 8d). This sudden ‘jump’ suggests a super-linear response of sea-ice edge
346 in the Northern Hemisphere to three Greenland melt-rates. With Antarctic meltwater, the sea-ice
347 edge migrates northward gradually (Fig. 8h), but it cannot move too far north due to the presence
348 of warm surface waters: it is found at 61°S, 59°S and 58.8°S in the 500 Gt yr⁻¹, 2000 Gt yr⁻¹ and



334 FIG. 7. Sea-ice coverage anomalies (%) averaged over 50 years for a, c, e) the Northern Hemisphere (NH)
 335 in the Greenland scenario and b, d, f) the Southern Hemisphere (SH) in the Antarctic scenario with meltwater
 336 forcings of 500 Gt yr⁻¹, 2000 Gt yr⁻¹ and 5000 Gt yr⁻¹, respectively. Purple contours indicate the Greenland
 337 and Antarctic areas where meltwater is fluxed into the ocean. Negative and positive values indicate the sea-ice
 338 expansion and retreat, respectively. The NH (north of 45°N) and SH (south of 45°S) averages of sea-ice coverage
 339 anomalies (with one standard deviation for ten ensemble members in the 500 Gt yr⁻¹ case) are indicated in the
 340 boxes in the bottom right of each panel.



351 FIG. 8. Hovmöller diagram of the zonal-mean sea-ice coverage (%) over 50 years for a, b, c) the NH in the
 352 Greenland scenario and e, f, g) the SH in the Antarctic scenario with meltwater forcings of 500 Gt yr⁻¹, 2000 Gt
 353 yr⁻¹ and 5000 Gt yr⁻¹, respectively. The zonal-mean sea-ice coverage anomalies (%) averaged over 50 years for
 354 d) the NH in the Greenland scenario and h) the SH in the Antarctic scenario. Contours in a-c) and e-g) indicate
 355 the latitude of maximum (marked in white) and 15 percent (black) sea-ice concentration after an 11-year moving
 356 average.

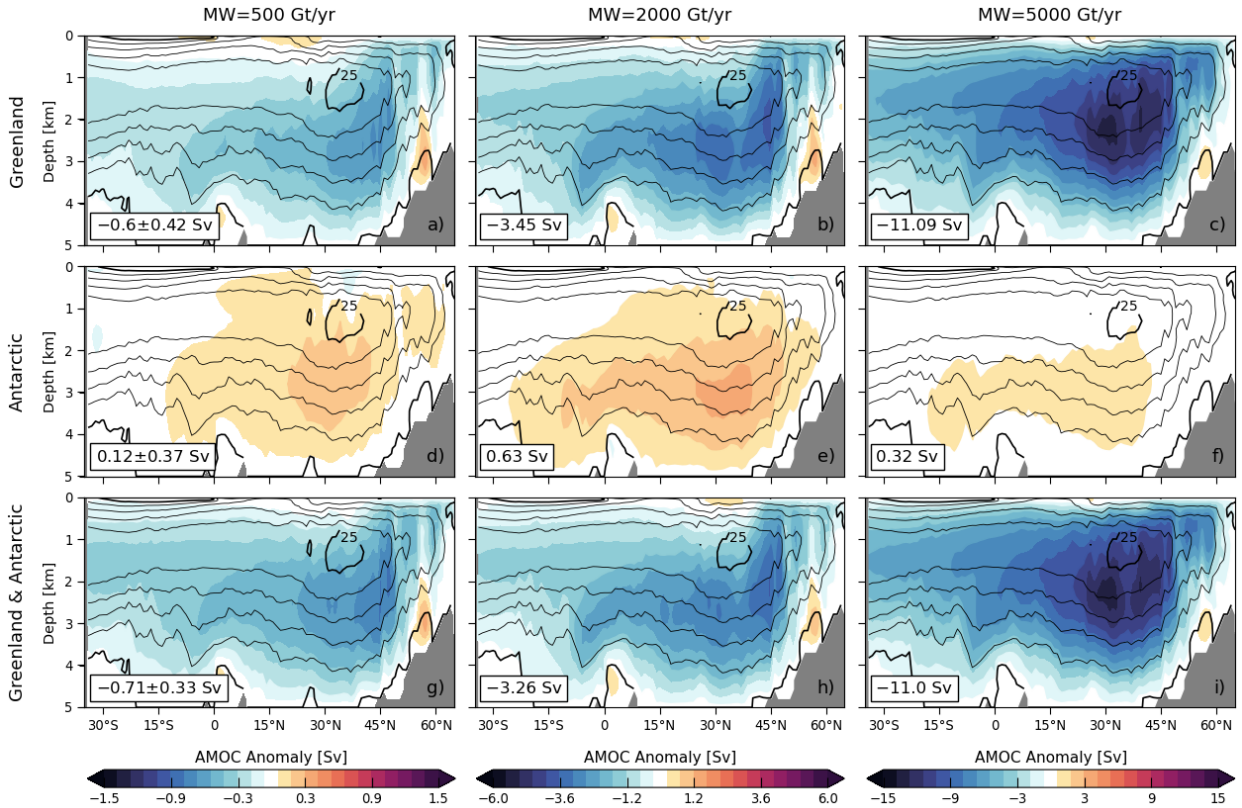
349 5000 Gt yr⁻¹ cases, respectively (Figs. 8e-g). This constrained Antarctic sea-ice edge, with a north
 350 limit of ~59°S, indicates a sub-linear response to three Antarctic melt-rates.

357 *b. AMOC response*

358 Another important mechanism is the influence of meltwater on the AMOC strength, which largely
359 controls the magnitude of cross-equatorial heat transport and hence the asymmetric temperature
360 response (Delworth et al. 1993; Stouffer et al. 2007; Marshall et al. 2014; Buckley and Marshall
361 2016). Here we define the AMOC strength as the maximum Atlantic overturning streamfunction
362 at 45°N. Greenland meltwater contributes to a pronounced AMOC decline (Fig. 9a-c), which is
363 in agreement with a recent observation-based inference (Rahmstorf et al. 2015) and many other
364 modeling studies (Caesar et al. 2018; Thornalley et al. 2018; Boers 2021). The degree of AMOC
365 decline is sensitive to Greenland melt-rates, and the response is non-linear. As Greenland melt-
366 rates increase to 5000 Gt yr⁻¹, the AMOC strength decreases by a remarkable ~50% (-11.09 Sv)
367 in 50 years (Fig. 9c). However, the AMOC strength is relatively insensitive to Antarctic melt-rates
368 (Fig. 9d-f), increasing by only 0.32 Sv in the 5000 Gt yr⁻¹ case (Fig. 9f)¹. When both Greenland
369 and Antarctic forcings are operative, the AMOC response is dominated by Greenland meltwater
370 and shows a decline much as found when Greenland-only forcing is operative (Figs. 9g-i)

371 We further show the temporal evolution of AMOC strength in Fig. 10. To examine the long-term
372 variability of the AMOC, all the simulations are extended out to 150 years. With the two large
373 meltwater forcings of 2000 Gt yr⁻¹ and 5000 Gt yr⁻¹, the AMOC overall transits to another steady
374 state with some fluctuations but with reduced amplitude in about 50 years. With the Greenland
375 melt-rate of 2000 Gt yr⁻¹, the AMOC strength weakens by ~19.5% (-4.38 Sv) in 150 years, which
376 turns out to be not sufficient for a critical transition point to collapse (Fig. 10a). As Greenland
377 melt-rates increase to 5000 Gt yr⁻¹, the AMOC eventually collapses (Fig. 10a). In contrast, with
378 Antarctic meltwater, the AMOC anomaly exhibits more frequent fluctuations, and these fluctuations
379 dampen down over time (Fig. 10b). Again, the variability of AMOC strength is dominated by
380 Greenland meltwater (Fig. 10c).

¹Weaver et al. (2003) argue that a change in the potential density relationship between the inflow of fresh Antarctic Intermediate Water (AAIW) and NADW can lead to enhanced formation of NADW and thence the AMOC.

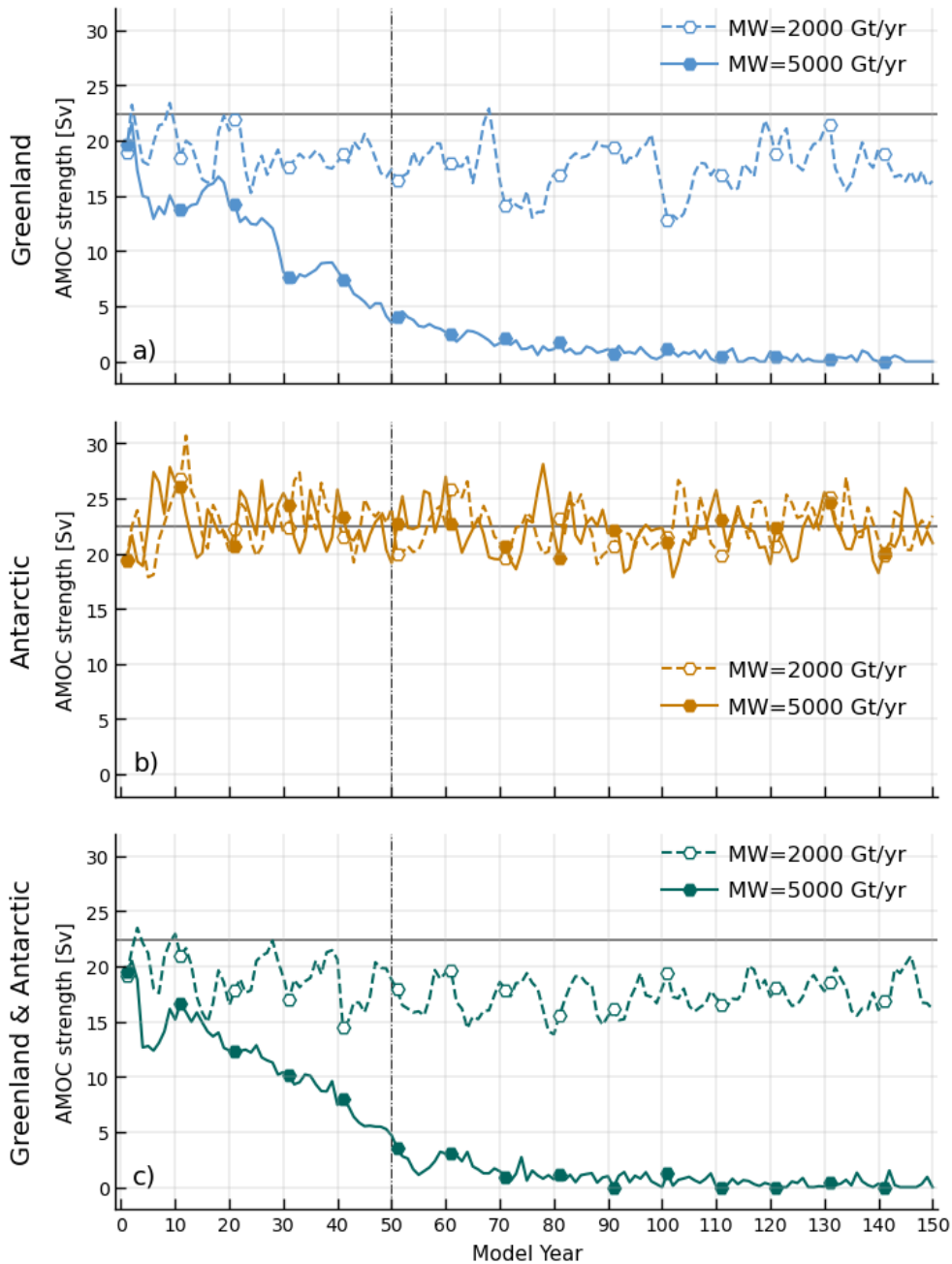


371 FIG. 9. Vertical cross-sections of the zonal-mean AMOC anomalies (Sv; color) averaged over 50 years in the
 372 a, b, c) Greenland, d, e, f) Antarctic and g, h, i) simultaneous Greenland and Antarctic scenarios with meltwater
 373 forcings of 500 Gt yr⁻¹, 2000 Gt yr⁻¹ and 5000 Gt yr⁻¹, respectively. Contours represent the climatological-mean
 374 AMOC with an interval of 5 Sv and values of 0 Sv and 5 Sv in bold from the control runs. The AMOC strength
 375 anomalies (with one standard deviation for ten ensemble members in the 500 Gt yr⁻¹ case) are indicated in the
 376 boxes in the bottom right of each panel.

392 5. Response functions for meltwater forcing

393 a. Climate response functions

394 Figure 11 shows the time series and fitted CRF curves of anomalies in the surface air temperature,
 395 sea-ice extent, AMOC strength and AABW transport, all scaled per unit forcing. Here we define
 396 the AABW transport as the magnitude of the minimum global overturning streamfunction between
 397 40°S and 50°S, which also reflects the strength of the lower cell. Plotted in this way, curves fall on
 398 top of one-another if the response scales linearly with the forcing amplitude moving from 500 Gt
 399 yr⁻¹, 2000 Gt yr⁻¹ to 5000 Gt yr⁻¹. Analytical CRF curves are superimposed and constructed to fit



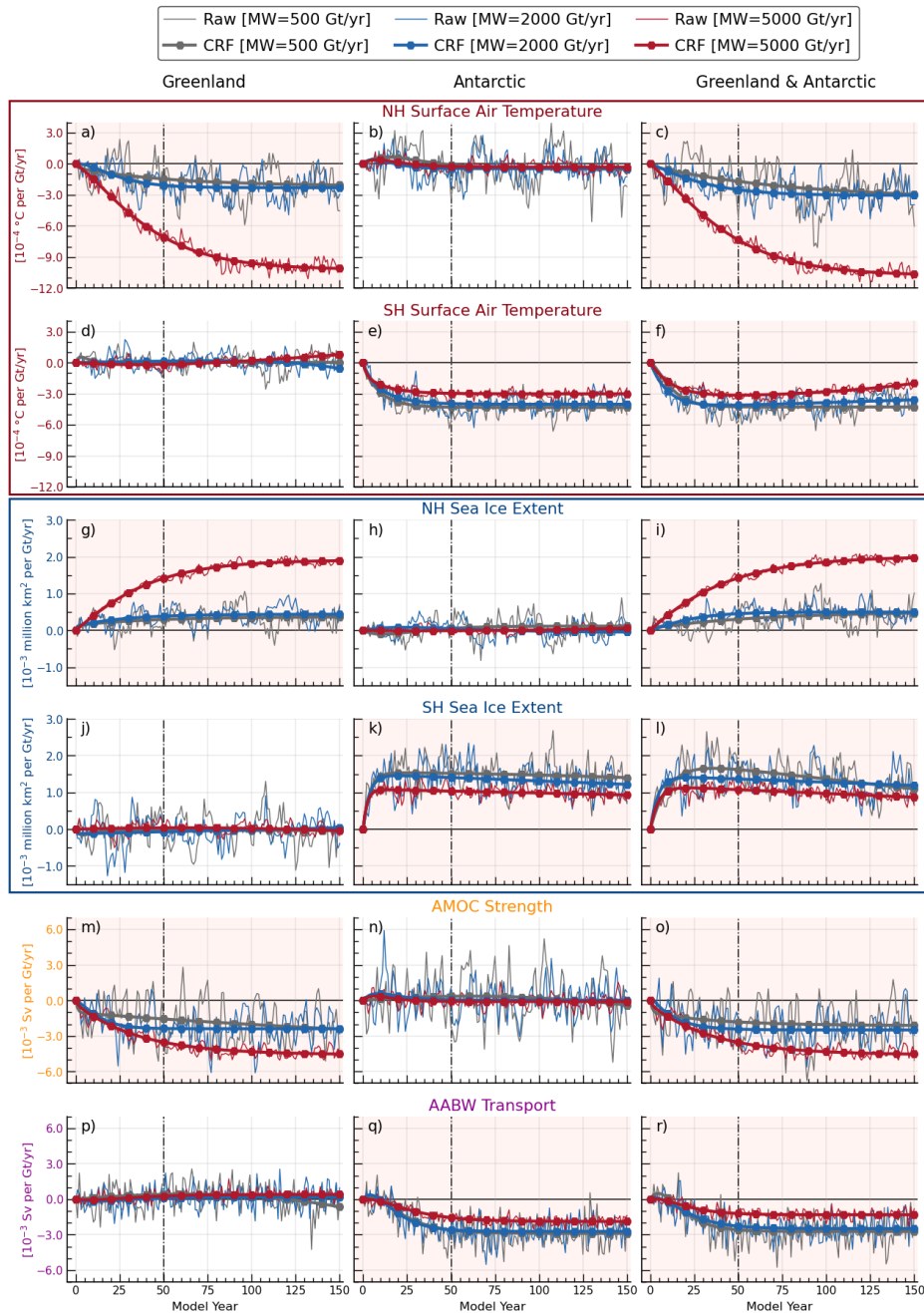
387 FIG. 10. Time series of the AMOC strength (Sv) in the a) Greenland (blue), b) Antarctic (orange) and c)
 388 simultaneous Greenland and Antarctic (green) scenarios with meltwater forcings of 2000 Gt yr⁻¹ (dashed line
 389 with hollow circles) and 5000 Gt yr⁻¹ (solid line with filled circles). Hollow and filled circles highlight the values
 390 every 10 years. The gray line denotes the climatological-mean AMOC strength of 22.45 Sv averaged over 150
 391 years from the control run.

400 the ensemble-means. Following Marshall et al. (2014), the fitted curves are calculated as the sum
401 of two exponential functions corresponding to a ‘fast’ and ‘slow’ response, expressed as:

$$CRF \times F_{step} = T_f \left(1 - e^{-t/\tau_f}\right) + T_s \left(1 - e^{-t/\tau_s}\right), \quad (1)$$

402 where F_{step} (in Gt yr^{-1}) is the scaling factor representing the magnitude of the step-function in
403 meltwater forcing, T_f and τ_f are the coefficients for the fast response, T_s and τ_s for the slow
404 response, and t is the time in years.

405 From Fig. 11, we see that the CRFs of surface air temperature and sea-ice extent anomalies
406 have a similar form in their respective hemispheres. For instance, with melt-rates of 500 Gt yr^{-1}
407 and 2000 Gt yr^{-1} , the CRFs of surface cooling and sea-ice expansion show a linear response to
408 Greenland meltwater in the Northern Hemisphere (Figs. 11a and 11g) and to Antarctic meltwater
409 in the Southern Hemisphere (Figs. 11e and 11k). At these two forcing levels, the hemispheric
410 response to Antarctic meltwater is greater than that to Greenland meltwater. However, with the
411 Greenland melt-rate of 5000 Gt yr^{-1} , we observe massive surface cooling and sea-ice expansion
412 in the Northern Hemisphere, leading to a super-linear response (Figs. 11a and 11g). This is a
413 consequence of a dramatic decline and indeed collapse of the AMOC (Figs. 10a and 11m). In
414 contrast, with the Antarctic melt-rate of 5000 Gt yr^{-1} , the response of surface cooling and sea-ice
415 expansion in the Southern Hemisphere is sub-linear (Figs. 11e and 11k). This sub-linear response
416 is likely due to the fact that the sea-ice edge cannot push further north of $\sim 59^\circ\text{S}$ (Figs. 8e-g), where
417 surface waters out in the open ocean are too warm to sustain ice. Furthermore, Antarctic meltwater
418 drives a significant reduction in AABW transport, analogous to the AMOC decline with Greenland
419 meltwater. The CRFs of AABW transport anomalies also show a sub-linear response to Antarctic
420 meltwater (Fig. 11q). Finally, by comparing with the CRFs in the simultaneous Greenland and
421 Antarctic scenario, we see that Greenland and Antarctica meltwater plays the dominant role in their
422 respective hemispheres (Fig. 11). The CRFs of all these climate parameters have no significant
423 and persistent response in the other hemisphere, and thus are set to zero in the fitted curves (Figs.
424 11b, 11d, 11h, 11j, 11n and 11p).



425 FIG. 11. Time series (dashed) and fitted curves, representing the CRFs (solid) of anomalies in the a, b, c) NH
 426 and d, e, f) SH surface air temperature ($^{\circ}\text{C}$ per Gt yr^{-1}), g, h, i) NH and j, k, l) SH sea-ice extent (million km^2
 427 per Gt yr^{-1}), m, n, o) AMOC strength (Sv per Gt yr^{-1}) and p, q, r) AABW transport (Sv per Gt yr^{-1}). Note that
 428 all curves are scaled per unit forcing for meltwater forcings of 500 Gt yr^{-1} (gray), 2000 Gt yr^{-1} (blue) and 5000
 429 Gt yr^{-1} (red), respectively. Analytical CRF curves are based on an exponential fit of raw time series. Light pink
 430 and white background shadings denote the significant (and persistent) and non-significant (close to a zero-line)
 431 CRFs, respectively. The NH and SH are defined as the region north of 23.5°N and south of 23.5°S , respectively,
 432 and thus exclude the tropics.

433 *b. Projections based on linear convolution theory*

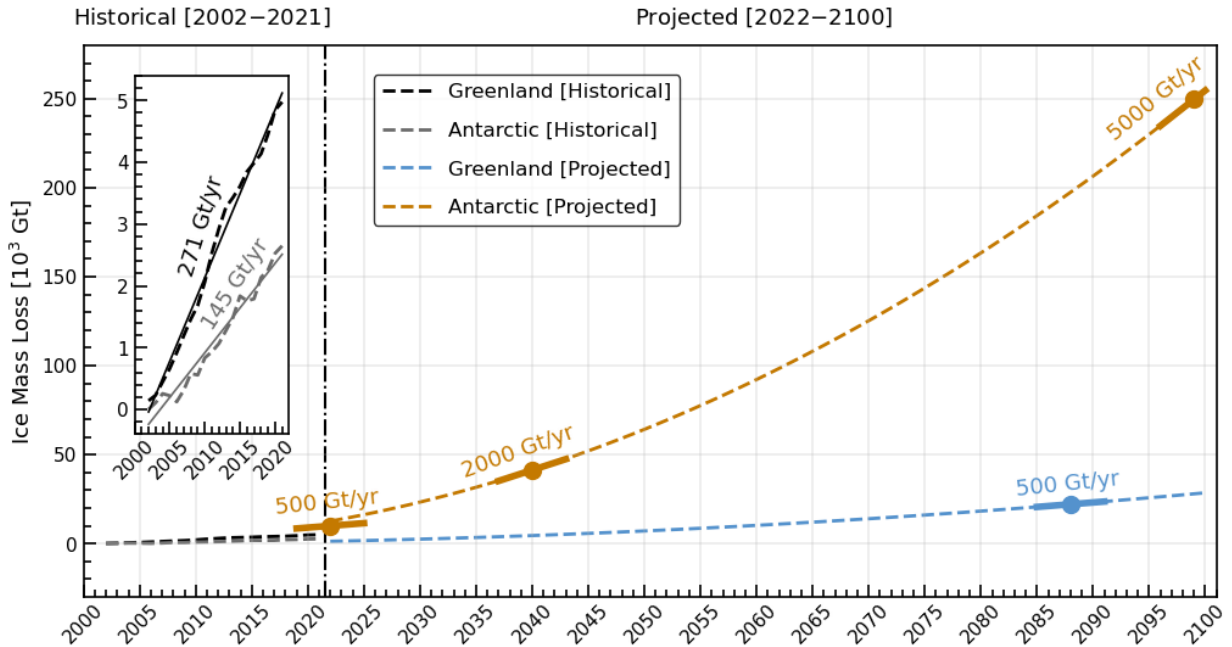
434 By applying linear convolution theory, as set out in previous studies (Hasselmann et al. 1993;
435 Marshall et al. 2014, 2017a), we can make projections of climate parameters of interest (\mathcal{P}) given
436 a postulated time series of meltwater forcing perturbation, thus:

$$\mathcal{P}(t) = \int_0^t CRF|_{\mathcal{P}}(t-t') \frac{\partial F}{\partial t}(t') dt', \quad (2)$$

437 where F (in Gt yr^{-1}) is the prescribed time-series of meltwater forcing perturbation, $CRF|_{\mathcal{P}}$ (scaled
438 per unit forcing) is the transient response of climate parameters to a step-change in meltwater
439 forcing, and t is the time in years.

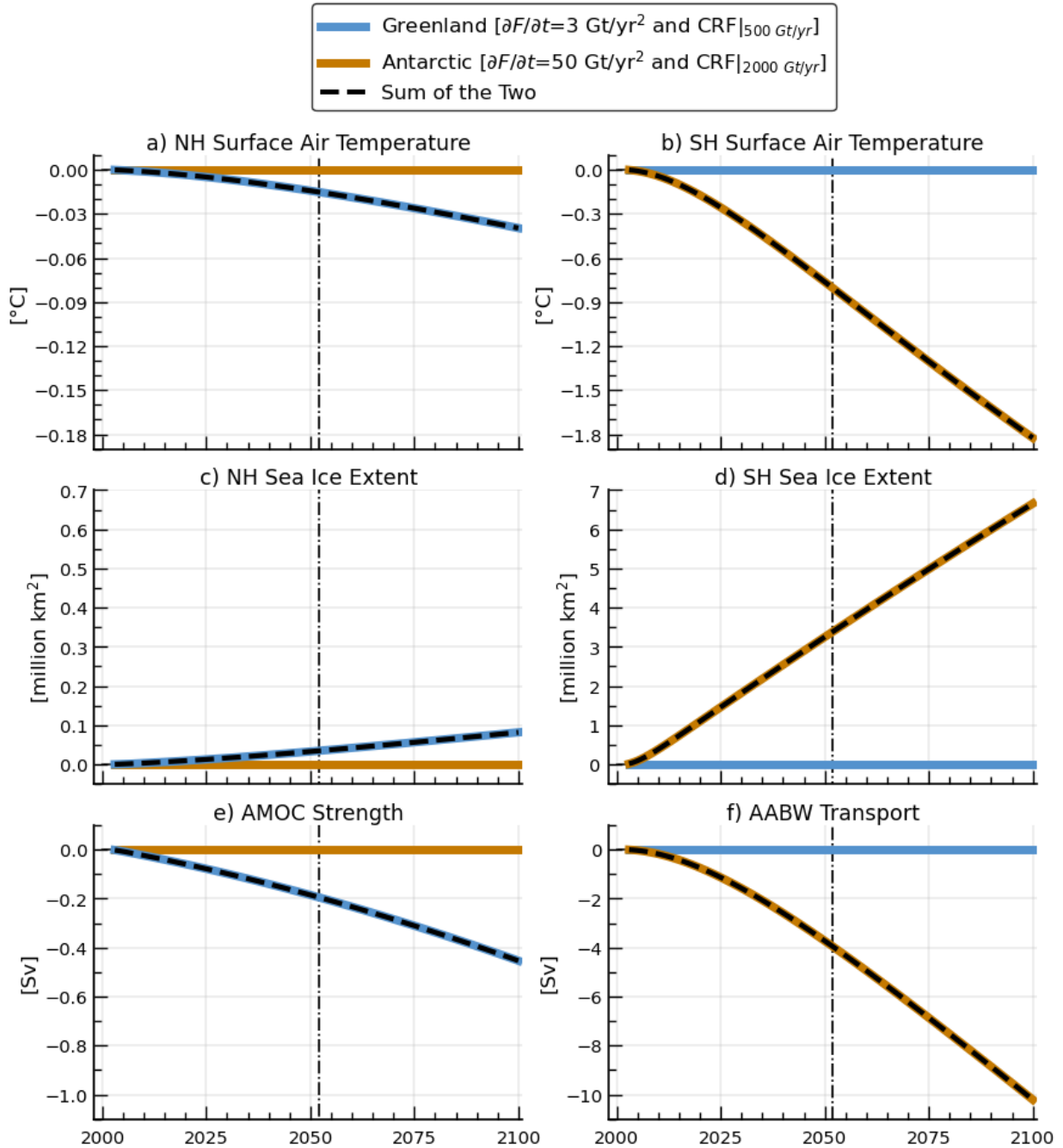
440 To make a projection, we first assume that the climate response depends linearly on meltwater
441 forcing, which we have shown to be valid in scenarios with small to moderate meltwater forcings.
442 In addition, we must assume a forcing function $F(t)$ and its time-derivative ($\partial F/\partial t$) — required
443 in Eq. (2) — for both Greenland and Antarctic meltwater. Ice mass loss-rates of both Greenland
444 and Antarctic ice sheets have been accelerating over recent decades: we estimate them using a
445 linear regression based on satellite gravity observation since 2002 (Watkins et al. 2015). During
446 the historical period 2002–2021, we find the loss-rates ($F|_{2002}$) to be 271 Gt yr^{-1} for Greenland and
447 145 Gt yr^{-1} for Antarctica (Fig. 12). Following the estimates based on the ice sheet simulations
448 of Golledge et al. (2019), we assume the loss-rates in 2100 ($F|_{2100}$) to be 568 Gt yr^{-1} (0.018 Sv)
449 for Greenland and 5047 Gt yr^{-1} (0.16 Sv) for Antarctica (Fig. 12). Using the loss-rates in 2002
450 ($F|_{2002}$) and 2100 ($F|_{2100}$), we obtain a gross estimate for a linear increase in forcing, yielding the
451 constant time-derivatives ($\partial F/\partial t$) of 3 Gt yr^{-2} for Greenland and 50 Gt yr^{-2} for Antarctica. The
452 $\partial F/\partial t$ is then used to carry out the integral in Eq. (2) after multiplying by the appropriate CRFs.
453 We also assume that ice mass loss in the ice sheet results in net fluxes of meltwater to the proximal
454 ocean. Note that over the twenty-first century, Antarctic melt-rates range from 500 Gt yr^{-1} through
455 2000 Gt yr^{-1} to 5000 Gt yr^{-1} , reaching a level that is almost one order of magnitude greater than
456 the Greenland melt-rate of 500 Gt yr^{-1} .

464 Figure 13 presents projections of climate parameters in response to Greenland and Antarctic
465 meltwater, both separately and together, so that we can better contrast their relative contributions.
466 We use the CRFs appropriate to the 500 Gt yr^{-1} curve for Greenland meltwater and 2000 Gt yr^{-1}



457 FIG. 12. Greenland (black and blue) and Antarctic (gray and orange) ice mass loss anomalies (Gt; dashed)
 458 relative to 2002 during the historical period 2002–2021 (Watkins et al. 2015) and projected forward from 2022–
 459 2100 under a high-emission scenario (Golledge et al. 2019). The inset box is a zoom on the historical period:
 460 the solid lines represent a linear regression of historical anomalies, yielding the constant loss-rates of 271 Gt yr⁻¹
 461 for Greenland (black) and 145 Gt yr⁻¹ for Antarctica (gray). During the remainder of the twenty-first century, the
 462 projected loss-rates reach 500 Gt yr⁻¹ around 2090 for Greenland (blue), and 500 Gt yr⁻¹, 2000 Gt yr⁻¹ and 5000
 463 Gt yr⁻¹ around 2025, 2040 and 2100 for Antarctica (orange), respectively.

467 curve for Antarctic meltwater. Consistent with our detailed calculations using the full model,
 468 Antarctic meltwater dominates in the Southern Hemisphere, inducing anomalous surface cooling,
 469 sea-ice expansion, and AABW contraction (Figs. 13b, 13d and 13f). Greenland meltwater
 470 dominates in the Northern Hemisphere, but anomalous surface cooling and sea-ice expansion are
 471 roughly one to two orders of magnitude smaller (Figs. 13a and 13c). Moreover, our projections
 472 suggest that by 2100, Greenland meltwater will cause only a small reduction of 0.45 Sv or so in
 473 AMOC strength (Fig. 13e), but Antarctic meltwater will induce a great reduction of 10.2 Sv in
 474 AABW transport (Fig. 13f). Such a marked reduction in AABW production could play a key role
 475 in abyssal ocean warming, as suggested in recent studies (Purkey and Johnson 2010; Li et al. 2022).



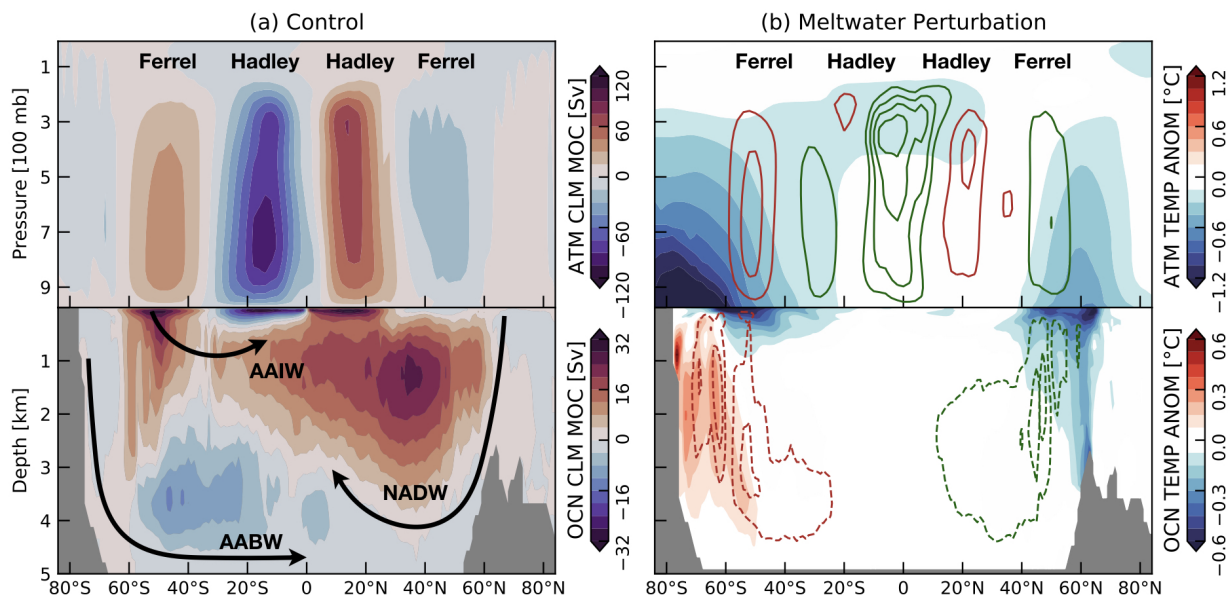
476 FIG. 13. Projections based on linear convolution for anomalies in the a) NH and b) SH surface air temperature
 477 (°C), c) NH and d) SH sea-ice extent (million km²), e) AMOC strength (Sv) and f) AABW transport (Sv).
 478 The blue (orange) solid line represents the projection assuming $\partial F/\partial t=3$ Gt yr⁻² (50 Gt yr⁻²) using the CRF
 479 appropriate to the 500 Gt yr⁻¹ (2000 Gt yr⁻¹) curve for Greenland (Antarctic) meltwater. The black dashed line
 480 represents the sum of two separate projections.

481 **6. Conclusions and discussion**

482 Greenland and Antarctic ice sheets have been melting and are likely to continue to melt at an
483 accelerating rate over the twenty-first century (Fox-Kemper et al. 2021). Meltwater injection into
484 the polar oceans is shown to have multiple significant large-scale climate impacts. These impacts
485 express hemispheric asymmetries due to geographical differences that drive distinct feedback
486 processes and response mechanisms. In this study, using a fully coupled climate model, we have
487 conducted nine step-function meltwater perturbation experiments, ranging from 500 Gt yr⁻¹ through
488 2000 Gt yr⁻¹ to 5000 Gt yr⁻¹ for Greenland and Antarctica, both separately and together. This has
489 enabled us to explore and contrast the global impacts of Greenland and Antarctic meltwater on the
490 climate system.

491 A broad summary of the changes induced by meltwater discharges is shown in Fig. 14. In
492 the atmosphere, ice-sheet meltwater from both hemispheres can cause significant changes in
493 temperature and circulation, such as cooling from the surface to the tropopause and strengthened
494 Ferrel and Hadley cells (Fig. 14b, top panel). For melt-rates up to 2000 Gt yr⁻¹, the Antarctic-
495 meltwater-driven changes are greater in magnitude and across a wider latitudinal extent. In
496 the ocean, Greenland meltwater weakens the upper cell and NADW formation, associated with
497 anomalous subsurface ocean cooling in the northern high-latitudes. Instead, Antarctic meltwater
498 slows down the lower cell and AABW formation, associated with anomalous subsurface ocean
499 warming around Antarctica (Fig. 14b, bottom panel). It should be noted that subsurface warming
500 around Antarctica could further accelerate the basal melt of ice shelves (Pritchard et al. 2012;
501 Rintoul et al. 2016), which has not been addressed in the present study.

515 Mechanisms controlling the climate response to Greenland and Antarctic meltwater are distinct.
516 Antarctic meltwater drives surface cooling and sea-ice expansion across the Southern Hemisphere,
517 by suppressing upper-ocean vertical heat exchange and positive ice-albedo feedback. A global-scale
518 atmospheric cooling can further develop by reducing the water vapor transfer from the southern
519 high-latitudes to the tropics (Rye et al. 2022). The climate response is rather linear for Antarctic
520 melt-rates up to 2000 Gt yr⁻¹, but ultimately becomes sub-linear with the larger melt-rate of 5000
521 Gt yr⁻¹. This is caused by the constrained sea-ice edge, as the continued expansion of sea ice
522 outward is capped by the presence of warm waters to the north. In contrast, with Greenland
523 meltwater, surface cooling and sea-ice expansion are more geographically confined in the Northern



502 FIG. 14. Summary figure showing the climate response to Greenland and Antarctic meltwater: a) the
 503 climatological state of the atmosphere (top panel) and ocean (bottom panel), and b) changes in key quantities.
 504 Key circulation patterns are also labeled and indicated by arrows. Green contours indicate anticlockwise
 505 circulation; red contours clockwise circulation. Continuous contours indicate a strengthening of the preexisting
 506 circulation; dashed contours a weakening. Quantities plotted are vertical cross-sections of the zonal-mean
 507 a) climatological-mean MOC (Sv; color) of the atmosphere (top panel) and ocean (bottom panel) from the
 508 control run, and b) anomalies in temperature (°C; color) and MOC (Sv; color-coded contours) of the atmosphere
 509 (top panel) and ocean (bottom panel) averaged over 50 years from the simultaneous Greenland and Antarctic
 510 perturbation experiment with meltwater forcing of 2000 Gt yr^{-1} . Dark green and deep red solid contours in the
 511 top panel of b) respectively show the negative and positive values of atmospheric MOC anomalies from -2.4 Sv
 512 to 1.2 Sv with an interval of 0.6 Sv: these represent *strengthened* Hadley and Ferrel cells. Dark green and deep
 513 red dashed contours in the bottom panel of b) show the negative and positive values of ocean MOC anomalies
 514 from -3 Sv to 3 Sv with an interval of 1.5 Sv: these represent *weakened* upper and lower cells.

524 Hemisphere. There seem to be two reasons: First, sea-ice expansion is bounded to a smaller
 525 geographic area in longitude; Second, surface cooling is also modulated by the AMOC slowdown,
 526 which reduces the poleward heat transport to the northern high-latitudes, with warming at lower
 527 latitudes that might counteract any reduced tropical cooling induced by water vapor. Moreover, the
 528 AMOC declines gradually for Greenland melt-rates up to 2000 Gt yr^{-1} , but eventually collapses

529 with the larger melt-rate of 5000 Gt yr⁻¹. The AMOC collapse causes dramatic atmospheric
530 and ocean changes: the climate response becomes amplifying and super-linear in the Northern
531 Hemisphere. Note that the super-linear response of sea-ice expansion is also related to its own
532 ‘threshold’ nature. As Greenland melt-rates increase to 5000 Gt yr⁻¹, sea ice moves sufficiently
533 further south to a large area, where the sea surface temperatures are below the freezing point of
534 seawater. Thus, once seawater freezes in that area allowing for greater effects on albedo and water
535 vapor, surface cooling produces additional sea ice much more rapidly and super-linearly.

536 Finally, we contrast the relative contributions of Greenland and Antarctic meltwater through
537 the analyses of CRFs and convolutions. Although Greenland dominates over Antarctic in the
538 historical period (Shepherd et al. 2018, 2020), Antarctic melt-rate is projected to be at least one
539 order of magnitude larger by 2100 (Golledge et al. 2019), due to its significant ice shelf-ocean
540 interactions. Our results suggest that as the century proceeds, Antarctic meltwater will largely
541 affect changes across the Southern Hemisphere, inducing anomalous surface cooling, sea-ice
542 expansion, and AABW contraction. By comparison, Greenland meltwater will still dominate the
543 climate response across the Northern Hemisphere, but with a much smaller magnitude. In this
544 assessment, the projected melt-rates are referenced to Golledge et al. (2019) under a high-emission
545 scenario. This represents an upper bound on what might be possible. For this upper bound, the
546 ‘non-linearity’ comes into effect early and, according to our analysis, the projected changes could
547 be relatively large. Yet there remain many uncertainties in estimates of projected melt-rates. For
548 instance, Golledge et al. (2019) presented ice-volume projections using initial conditions from
549 coarse-resolution CMIP5 models. These models cannot accurately represent fine-scale processes,
550 such as the waters that interact with the Antarctic shelf (Purich and England 2021). In addition,
551 DeConto and Pollard (2016) also projected an ice-sheet retreat but with a much larger melt-rate of
552 15,800 Gt yr⁻¹ (~0.5 Sv) for Antarctica in 2100 (see their Extended Data Fig. 8).

553 The goal of our study is to assess the climate impacts of ice-sheet meltwater, and we therefore
554 employ a fully coupled climate model. While our model simulates distinct freshwater pathways
555 around Greenland and Antarctica, the ~1° horizontal resolution of our ocean model excludes
556 mesoscale eddies and small-scale topographic features, which influence western boundary currents
557 tight to the coast of the Labrador Sea (Gillard et al. 2016), shelf circulation and dense water
558 formation around the Antarctic margins (Thompson et al. 2018; Morrison et al. 2020). In our

559 model, most of the NADW formation is produced from the Labrador and Irminger Seas, much less
560 from the GIN Seas than observed (Pickart and Spall 2007; Lozier et al. 2019), probably because the
561 Iceland-Faroe Islands sills are too shallow to allow the dense water to spill into the North Atlantic.
562 Our model simulates an AMOC that is somewhat stronger than observed (Miller et al. 2021), with
563 a relatively rapid decline of the AMOC among CMIP6 models in response to global warming
564 (Bellomo et al. 2021). In the context of this study, we detect some slight inter-hemispheric climate
565 linkages driven by Antarctic meltwater, such as the abyssal warming extending across the equator
566 after 50 years and ocean cooling in the north after 100 years (not shown). However, we do not find
567 a clear response of the AMOC to Antarctic meltwater, which may be due to the limited duration of
568 our experiments extending out to only 150 years. Despite the above caveats, our results robustly
569 contrast the role of Greenland vs. Antarctic meltwater in instigating global climate change.

570 *Acknowledgments.* QL, JM, CR and AR are supported by the NASA MAP program 19-MAP19-
571 0011 and the MIT-GISS cooperative agreement. The model simulations and analysis were con-
572 ducted on the NASA High-End Computing (HEC) Program through the NASA Center for Climate
573 Simulation (NCCS) at Goddard Space Flight Center.

574 *Data availability statement.* The data sets analyzed in this study will be all publicly avail-
575 able. Model components are all open source. The GISS modelE is available at <https://www.giss.nasa.gov/tools/modelE/>. The Greenland and Antarctic ice mass data from
576 satellite observations were obtained for the period 2002–2021 at <https://climate.nasa.gov/vital-signs/ice-sheets/>.

579 **References**

- 580 Adusumilli, S., H. A. Fricker, B. Medley, L. Padman, and M. R. Siegfried, 2020: Interannual vari-
581 ations in meltwater input to the Southern Ocean from Antarctic ice shelves. *Nature Geoscience*,
582 **13 (9)**, 616–620, <https://doi.org/10.1038/s41561-020-0616-z>.
- 583 Bakker, P., and M. Prange, 2018: Response of the intertropical convergence zone to Antarctic ice
584 sheet melt. *Geophysical Research Letters*, **45 (16)**, 8673–8680, <https://doi.org/https://doi.org/10.1029/2018GL078659>.
- 586 Bakker, P., and Coauthors, 2016: Fate of the Atlantic Meridional Overturning Circulation: Strong
587 decline under continued warming and Greenland melting. *Geophysical Research Letters*, **43 (23)**,
588 12,252–12,260, <https://doi.org/https://doi.org/10.1002/2016GL070457>.
- 589 Beadling, R. L., and Coauthors, 2022: Importance of the antarctic slope current in the southern
590 ocean response to ice sheet melt and wind stress change. *Journal of Geophysical Research: Oceans*,
591 **127 (5)**, e2021JC017 608, <https://doi.org/https://doi.org/10.1029/2021JC017608>.
- 592 Bellomo, K., M. Angeloni, S. Corti, and J. von Hardenberg, 2021: Future climate change shaped
593 by inter-model differences in Atlantic meridional overturning circulation response. *Nature com-*
594 *munications*, **12 (1)**, 3659–3659, <https://doi.org/10.1038/s41467-021-24015-w>.
- 595 Bintanja, R., G. J. van Oldenborgh, S. S. Drijfhout, B. Wouters, and C. A. Katsman, 2013:
596 Important role for ocean warming and increased ice-shelf melt in Antarctic sea-ice expansion.
597 *Nature Geoscience*, **6 (5)**, 376–379, <https://doi.org/10.1038/ngeo1767>.
- 598 Bitz, C. M., and W. H. Lipscomb, 1999: An energy-conserving thermodynamic model of sea
599 ice. *Journal of Geophysical Research: Oceans*, **104 (C7)**, 15 669–15 677, <https://doi.org/https://doi.org/10.1029/1999JC900100>.
- 601 Boers, N., 2021: Observation-based early-warning signals for a collapse of the atlantic merid-
602 ional overturning circulation. *Nature Climate Change*, **11 (8)**, 680–688, <https://doi.org/10.1038/s41558-021-01097-4>.
- 604 Böning, C. W., E. Behrens, A. Biastoch, K. J. Getzlaff, and J. L. Bamber, 2016: Emerging impact of
605 Greenland meltwater on deepwater formation in the North Atlantic Ocean. *Nature Geoscience*,
606 **9 (7)**, 523–527, <https://doi.org/10.1038/ngeo2740>.

607 Bronselaer, B., M. Winton, S. M. Griffies, W. J. Hurlin, K. B. Rodgers, O. V. Sergienko, R. J.
608 Stouffer, and J. L. Russell, 2018: Change in future climate due to Antarctic meltwater. *Nature*,
609 **564 (7734)**, 53–58, <https://doi.org/10.1038/s41586-018-0712-z>.

610 Buckley, M. W., and J. Marshall, 2016: Observations, inferences, and mechanisms of the At-
611 lantic Meridional Overturning Circulation: A review. *Reviews of Geophysics*, **54 (1)**, 5–63,
612 <https://doi.org/https://doi.org/10.1002/2015RG000493>.

613 Caesar, L., S. Rahmstorf, A. Robinson, G. Feulner, and V. Saba, 2018: Observed fingerprint of a
614 weakening Atlantic Ocean overturning circulation. *Nature*, **556 (7700)**, 191–196, <https://doi.org/10.1038/s41586-018-0006-5>.

615

616 Czaja, A., and J. Marshall, 2006: The partitioning of poleward heat transport between the at-
617 mosphere and ocean. *Journal of the Atmospheric Sciences*, **63 (5)**, 1498–1511, <https://doi.org/10.1175/JAS3695.1>.

618

619 DeConto, R. M., and D. Pollard, 2016: Contribution of Antarctica to past and future sea-level rise.
620 *Nature*, **531 (7596)**, 591–597, <https://doi.org/10.1038/nature17145>.

621 Delworth, T., S. Manabe, and R. J. Stouffer, 1993: Interdecadal variations of the thermohaline
622 circulation in a coupled ocean-atmosphere model. *Journal of Climate*, **6 (11)**, 1993–2011,
623 [https://doi.org/10.1175/1520-0442\(1993\)006<1993:IVOTTC>2.0.CO;2](https://doi.org/10.1175/1520-0442(1993)006<1993:IVOTTC>2.0.CO;2).

624 Depoorter, M. A., J. L. Bamber, J. A. Griggs, J. T. M. Lenaerts, S. R. M. Ligtenberg, M. R. van den
625 Broeke, and G. Moholdt, 2013: Calving fluxes and basal melt rates of Antarctic ice shelves.
626 *Nature*, **502 (7469)**, 89–92, <https://doi.org/10.1038/nature12567>.

627 Eyring, V., S. Bony, G. A. Meehl, C. A. Senior, B. Stevens, R. J. Stouffer, and K. E. Taylor,
628 2016: Overview of the Coupled Model Intercomparison Project Phase 6 (CMIP6) experimental
629 design and organization. *Geoscientific Model Development*, **9 (5)**, 1937–1958, <https://doi.org/10.5194/gmd-9-1937-2016>.

630

631 Fox-Kemper, B., and Coauthors, 2021: Ocean, cryosphere and sea level change. *Climate Change*
632 *2021: The Physical Science Basis. Contribution of Working Group I to the Sixth Assessment*
633 *Report of the Intergovernmental Panel on Climate Change*, V. Masson-Delmotte, P. Zhai, A. Pi-
634 rani, S. Connors, C. Péan, S. Berger, N. Caud, Y. Chen, L. Goldfarb, M. Gomis, M. Huang,

635 K. Leitzell, E. Lonnoy, J. Matthews, T. Maycock, T. Waterfield, O. Yelekçi, R. Yu, and B. Zhou,
636 Eds., Cambridge University Press, Cambridge, United Kingdom and New York, NY, USA,
637 chapter 9, 1211–1362, <https://doi.org/10.1017/9781009157896.011>.

638 Fretwell, P., and Coauthors, 2013: Bedmap2: improved ice bed, surface and thickness datasets for
639 Antarctica. *The Cryosphere*, **7 (1)**, 375–393, <https://doi.org/10.5194/tc-7-375-2013>.

640 Gent, P. R., J. Willebrand, T. J. McDougall, and J. C. McWilliams, 1995: Parameterizing eddy-
641 induced tracer transports in ocean circulation models. *Journal of Physical Oceanography*, **25 (4)**,
642 463–474, [https://doi.org/10.1175/1520-0485\(1995\)025<0463:PEITTI>2.0.CO;2](https://doi.org/10.1175/1520-0485(1995)025<0463:PEITTI>2.0.CO;2).

643 Gillard, L. C., X. Hu, P. G. Myers, and J. L. Bamber, 2016: Meltwater pathways from marine
644 terminating glaciers of the Greenland ice sheet. *Geophysical Research Letters*, **43 (20)**, 10,873–
645 10,882, <https://doi.org/https://doi.org/10.1002/2016GL070969>.

646 Golledge, N. R., E. D. Keller, N. Gomez, K. A. Naughten, J. Bernales, L. D. Trusel, and T. L.
647 Edwards, 2019: Global environmental consequences of twenty-first-century ice-sheet melt.
648 *Nature*, **566 (7742)**, 65–72, <https://doi.org/10.1038/s41586-019-0889-9>.

649 Gregory, J. M., T. Andrews, and P. Good, 2015: The inconstancy of the transient climate response
650 parameter under increasing co₂. *Philosophical Transactions of the Royal Society
651 A: Mathematical, Physical and Engineering Sciences*, **373 (2054)**, 20140417, [https://doi.org/
652 10.1098/rsta.2014.0417](https://doi.org/10.1098/rsta.2014.0417).

653 Hasselmann, K., R. Sausen, E. Maier-Reimer, and R. Voss, 1993: On the cold start problem in
654 transient simulations with coupled atmosphere-ocean models. *Climate Dynamics*, **9 (2)**, 53–61,
655 <https://doi.org/10.1007/BF00210008>.

656 Hellmer, H. H., 2004: Impact of Antarctic ice shelf basal melting on sea ice and deep
657 ocean properties. *Geophysical Research Letters*, **31 (10)**, [https://doi.org/https://doi.org/10.1029/
658 2004GL019506](https://doi.org/https://doi.org/10.1029/2004GL019506).

659 Hu, A., G. A. Meehl, W. Han, and J. Yin, 2011: Effect of the potential melting of the Greenland
660 ice sheet on the meridional overturning circulation and global climate in the future. *Deep
661 Sea Research Part II: Topical Studies in Oceanography*, **58 (17)**, 1914–1926, [https://doi.org/
662 https://doi.org/10.1016/j.dsr2.2010.10.069](https://doi.org/https://doi.org/10.1016/j.dsr2.2010.10.069).

- 663 Jayne, S. R., 2009: The impact of abyssal mixing parameterizations in an ocean general
664 circulation model. *Journal of Physical Oceanography*, **39** (7), 1756–1775, [https://doi.org/](https://doi.org/10.1175/2009JPO4085.1)
665 10.1175/2009JPO4085.1.
- 666 Kelley, M., and Coauthors, 2020: GISS-E2.1: Configurations and climatology. *Journal of Advances*
667 *in Modeling Earth Systems*, **12** (8), e2019MS002025, [https://doi.org/https://doi.org/10.1029/](https://doi.org/https://doi.org/10.1029/2019MS002025)
668 2019MS002025.
- 669 King, M. D., and Coauthors, 2020: Dynamic ice loss from the Greenland Ice Sheet driven
670 by sustained glacier retreat. *Communications Earth & Environment*, **1** (1), 1, [https://doi.org/](https://doi.org/10.1038/s43247-020-0001-2)
671 10.1038/s43247-020-0001-2.
- 672 Lago, V., and M. H. England, 2019: Projected slowdown of Antarctic Bottom Water formation
673 in response to amplified meltwater contributions. *Journal of Climate*, **32** (19), 6319–6335,
674 <https://doi.org/10.1175/JCLI-D-18-0622.1>.
- 675 Large, W. G., J. C. McWilliams, and S. C. Doney, 1994: Oceanic vertical mixing: A review
676 and a model with a nonlocal boundary layer parameterization. *Reviews of Geophysics*, **32** (4),
677 363–403, <https://doi.org/https://doi.org/10.1029/94RG01872>.
- 678 Lembo, V., V. Lucarini, and F. Ragone, 2020: Beyond forcing scenarios: Predicting climate change
679 through response operators in a coupled general circulation model. *Scientific Reports*, **10** (1),
680 8668, <https://doi.org/10.1038/s41598-020-65297-2>.
- 681 Lerner, P., A. Romanou, M. Kelley, J. Romanski, R. Ruedy, and G. Russell, 2021: Drivers of air-sea
682 CO₂ flux seasonality and its long-term changes in the NASA-GISS model CMIP6 submission.
683 *Journal of Advances in Modeling Earth Systems*, **13** (2), e2019MS002028, [https://doi.org/](https://doi.org/https://doi.org/10.1029/2019MS002028)
684 <https://doi.org/10.1029/2019MS002028>.
- 685 Li, Q., M. H. England, A. M. Hogg, S. R. Rintoul, and A. K. Morrison, 2022: Future abyssal ocean
686 warming driven by glacial melt. *Submitted*.
- 687 Lozier, M. S., and Coauthors, 2019: A sea change in our view of overturning in the subpolar North
688 Atlantic. *Science*, **363** (6426), 516–521, <https://doi.org/10.1126/science.aau6592>.

- 689 Mackie, S., I. J. Smith, J. K. Ridley, D. P. Stevens, and P. J. Langhorne, 2020: Climate response
690 to increasing Antarctic iceberg and ice shelf melt. *Journal of Climate*, **33** (20), 8917–8938,
691 <https://doi.org/10.1175/JCLI-D-19-0881.1>.
- 692 Marshall, J., K. C. Armour, J. R. Scott, Y. Kostov, U. Hausmann, D. Ferreira, T. G. Shepherd, and
693 C. M. Bitz, 2014: The ocean’s role in polar climate change: asymmetric Arctic and Antarctic
694 responses to greenhouse gas and ozone forcing. *Philosophical Transactions of the Royal Society
695 A: Mathematical, Physical and Engineering Sciences*, **372** (2019), 20130040, [https://doi.org/
696 10.1098/rsta.2013.0040](https://doi.org/10.1098/rsta.2013.0040).
- 697 Marshall, J., J. Scott, and A. Proshutinsky, 2017a: “Climate response functions” for the Arctic
698 ocean: a proposed coordinated modelling experiment. *Geoscientific Model Development*, **10** (7),
699 2833–2848, <https://doi.org/10.5194/gmd-10-2833-2017>.
- 700 Marshall, J., J. R. Scott, A. Romanou, M. Kelley, and A. Leboissetier, 2017b: The dependence of
701 the ocean’s MOC on mesoscale eddy diffusivities: A model study. *Ocean Modelling*, **111**, 1–8,
702 <https://doi.org/https://doi.org/10.1016/j.ocemod.2017.01.001>.
- 703 Marshall, J., and K. Speer, 2012: Closure of the meridional overturning circulation through South-
704 ern Ocean upwelling. *Nature Geoscience*, **5** (3), 171–180, <https://doi.org/10.1038/ngeo1391>.
- 705 Miller, R. L., and Coauthors, 2021: Cmp6 historical simulations (1850–2014) with GISS-E2.1.
706 *Journal of Advances in Modeling Earth Systems*, **13** (1), e2019MS002034, [https://doi.org/
707 https://doi.org/10.1029/2019MS002034](https://doi.org/https://doi.org/10.1029/2019MS002034).
- 708 Morlighem, M., and Coauthors, 2017: Bedmachine v3: Complete bed topography and
709 ocean bathymetry mapping of Greenland from multibeam echo sounding combined with
710 mass conservation. *Geophysical Research Letters*, **44** (21), 11,051–11,061, [https://doi.org/
711 https://doi.org/10.1002/2017GL074954](https://doi.org/https://doi.org/10.1002/2017GL074954).
- 712 Morrison, A. K., A. M. Hogg, M. H. England, and P. Spence, 2020: Warm Circumpolar Deep Water
713 transport toward Antarctica driven by local dense water export in canyons. *Science Advances*,
714 **6** (18), eaav2516, <https://doi.org/10.1126/sciadv.aav2516>.

- 715 Mougnot, J., and Coauthors, 2019: Forty-six years of Greenland ice sheet mass balance from 1972
716 to 2018. *Proceedings of the National Academy of Sciences*, **116 (19)**, 9239–9244, <https://doi.org/10.1073/pnas.1904242116>.
717
- 718 Nazarenko, L. S., and Coauthors, 2022: Future climate change under ssp emission scenarios
719 with giss-e2.1. *Journal of Advances in Modeling Earth Systems*, **In press**, e2021MS002871,
720 <https://doi.org/https://doi.org/10.1029/2021MS002871>.
- 721 Orihuela-Pinto, B., M. H. England, and A. S. Taschetto, 2022: Interbasin and interhemispheric
722 impacts of a collapsed Atlantic Overturning Circulation. *Nature Climate Change*, **In press**,
723 <https://doi.org/10.1038/s41558-022-01380-y>.
- 724 Paolo, F. S., H. A. Fricker, and L. Padman, 2015: Volume loss from Antarctic ice shelves is
725 accelerating. *Science*, **348 (6232)**, 327–331, <https://doi.org/10.1126/science.aaa0940>.
- 726 Pauling, A. G., C. M. Bitz, I. J. Smith, and P. J. Langhorne, 2016: The response of the Southern
727 Ocean and Antarctic sea ice to freshwater from ice shelves in an earth system model. *Journal of*
728 *Climate*, **29 (5)**, 1655–1672, <https://doi.org/10.1175/JCLI-D-15-0501.1>.
- 729 Pickart, R. S., and M. A. Spall, 2007: Impact of Labrador Sea convection on the North Atlantic
730 meridional overturning circulation. *Journal of Physical Oceanography*, **37 (9)**, 2207–2227,
731 <https://doi.org/10.1175/JPO3178.1>.
- 732 Prather, M. J., 1986: Numerical advection by conservation of second-order moments. *Journal*
733 *of Geophysical Research: Atmospheres*, **91 (D6)**, 6671–6681, <https://doi.org/https://doi.org/10.1029/JD091iD06p06671>.
734
- 735 Pritchard, H. D., S. R. M. Ligtenberg, H. A. Fricker, D. G. Vaughan, M. R. van den Broeke,
736 and L. Padman, 2012: Antarctic ice-sheet loss driven by basal melting of ice shelves. *Nature*,
737 **484 (7395)**, 502–505, <https://doi.org/10.1038/nature10968>.
- 738 Purich, A., and M. H. England, 2021: Historical and future projected warming of Antarctic Shelf
739 Bottom Water in CMIP6 models. *Geophysical Research Letters*, **48 (10)**, e2021GL092752,
740 <https://doi.org/https://doi.org/10.1029/2021GL092752>.

- 741 Purkey, S. G., and G. C. Johnson, 2010: Warming of global abyssal and deep Southern Ocean
742 waters between the 1990s and 2000s: Contributions to global heat and sea level rise budgets.
743 *Journal of Climate*, **23** (23), 6336–6351, <https://doi.org/10.1175/2010JCLI3682.1>.
- 744 Putrasahan, D. A., K. Lohmann, J.-S. von Storch, J. H. Jungclaus, O. Gutjahr, and H. Haak, 2019:
745 Surface flux drivers for the slowdown of the Atlantic Meridional Overturning Circulation in a
746 high-resolution global coupled climate model. *Journal of Advances in Modeling Earth Systems*,
747 **11** (5), 1349–1363, <https://doi.org/https://doi.org/10.1029/2018MS001447>.
- 748 Rahmstorf, S., J. E. Box, G. Feulner, M. E. Mann, A. Robinson, S. Rutherford, and E. J. Schaffer-
749 nicht, 2015: Exceptional twentieth-century slowdown in Atlantic Ocean overturning circulation.
750 *Nature Climate Change*, **5** (5), 475–480, <https://doi.org/10.1038/nclimate2554>.
- 751 Richardson, G., M. R. Wadley, K. J. Heywood, D. P. Stevens, and H. T. Banks, 2005: Short-term
752 climate response to a freshwater pulse in the southern ocean. *Geophysical Research Letters*,
753 **32** (3), <https://doi.org/https://doi.org/10.1029/2004GL021586>.
- 754 Rignot, E., S. Jacobs, J. Mouginot, and B. Scheuchl, 2013: Ice-shelf melting around Antarctica.
755 *Science*, **341** (6143), 266–270, <https://doi.org/10.1126/science.1235798>.
- 756 Rignot, E., J. Mouginot, B. Scheuchl, M. van den Broeke, M. J. van Wessem, and M. Morlighem,
757 2019: Four decades of Antarctic ice sheet mass balance from 1979–2017. *Proceedings of the*
758 *National Academy of Sciences*, **116** (4), 1095–1103, <https://doi.org/10.1073/pnas.1812883116>.
- 759 Rintoul, S. R., A. Silvano, B. Pena-Molino, E. van Wijk, M. Rosenberg, J. S. Greenbaum, and
760 D. D. Blankenship, 2016: Ocean heat drives rapid basal melt of the Totten Ice Shelf. *Science*
761 *Advances*, **2** (12), e1601610, <https://doi.org/10.1126/sciadv.1601610>.
- 762 Russell, G. L., J. R. Miller, and D. Rind, 1995: A coupled atmosphere-ocean model for transient
763 climate change studies. *Atmosphere-Ocean*, **33** (4), 683–730, [https://doi.org/10.1080/07055900.](https://doi.org/10.1080/07055900.1995.9649550)
764 1995.9649550.
- 765 Rye, C. D., J. Marshall, M. Kelley, G. Russell, L. S. Nazarenko, Y. Kostov, G. A. Schmidt,
766 and J. Hansen, 2020: Antarctic glacial melt as a driver of recent Southern Ocean climate
767 trends. *Geophysical Research Letters*, **47** (11), e2019GL086892, [https://doi.org/https://doi.org/](https://doi.org/https://doi.org/10.1029/2019GL086892)
768 [10.1029/2019GL086892](https://doi.org/10.1029/2019GL086892).

769 Rye, C. D., J. Marshall, D. Rind, G. A. Schmidt, and J. E. Hansen, 2022: Partial mitigation of
770 global warming through Antarctic meltwater anomalies. *Science Advances*, **In revision**.

771 Schmidt, G. A., and Coauthors, 2014: Configuration and assessment of the giss modele2 contri-
772 butions to the cmip5 archive. *Journal of Advances in Modeling Earth Systems*, **6 (1)**, 141–184,
773 <https://doi.org/https://doi.org/10.1002/2013MS000265>.

774 Shepherd, A., and Coauthors, 2018: Mass balance of the Antarctic ice sheet from 1992 to 2017.
775 *Nature*, **558 (7709)**, 219–222, <https://doi.org/10.1038/s41586-018-0179-y>.

776 Shepherd, A., and Coauthors, 2020: Mass balance of the Greenland ice sheet from 1992 to 2018.
777 *Nature*, **579 (7798)**, 233–239, <https://doi.org/10.1038/s41586-019-1855-2>.

778 Silvano, A., S. R. Rintoul, B. Peña-Molino, W. R. Hobbs, E. van Wijk, S. Aoki, T. Tamura, and
779 G. D. Williams, 2018: Freshening by glacial meltwater enhances melting of ice shelves and
780 reduces formation of Antarctic Bottom Water. *Science Advances*, **4 (4)**, eaap9467, <https://doi.org/10.1126/sciadv.aap9467>.

782 Stouffer, R. J., D. Seidov, and B. J. Haupt, 2007: Climate response to external sources of freshwater:
783 North Atlantic versus the Southern Ocean. *Journal of Climate*, **20 (3)**, 436–448, <https://doi.org/10.1175/JCLI4015.1>.

785 Thompson, A. F., A. L. Stewart, P. Spence, and K. J. Heywood, 2018: The Antarctic Slope
786 Current in a changing climate. *Reviews of Geophysics*, **56 (4)**, 741–770, <https://doi.org/https://doi.org/10.1029/2018RG000624>.

788 Thornalley, D. J. R., and Coauthors, 2018: Anomalously weak Labrador Sea convection and
789 Atlantic overturning during the past 150 years. *Nature*, **556 (7700)**, 227–230, <https://doi.org/10.1038/s41586-018-0007-4>.

791 Tournadre, J., N. Bouhier, F. Girard-Ardhuin, and F. Rémy, 2016: Antarctic icebergs distributions
792 1992–2014. *Journal of Geophysical Research: Oceans*, **121 (1)**, 327–349, <https://doi.org/https://doi.org/10.1002/2015JC011178>.

794 Visbeck, M., J. Marshall, T. Haine, and M. Spall, 1997: Specification of eddy transfer coefficients
795 in coarse-resolution ocean circulation models. *Journal of Physical Oceanography*, **27 (3)**, 381–
796 402, [https://doi.org/10.1175/1520-0485\(1997\)027<0381:SOETCI>2.0.CO;2](https://doi.org/10.1175/1520-0485(1997)027<0381:SOETCI>2.0.CO;2).

- 797 Watkins, M. M., D. N. Wiese, D.-N. Yuan, C. Boening, and F. W. Landerer, 2015: Improved
798 methods for observing Earth's time variable mass distribution with GRACE using spherical cap
799 mascons. *Journal of Geophysical Research: Solid Earth*, **120** (4), 2648–2671, [https://doi.org/
800 https://doi.org/10.1002/2014JB011547](https://doi.org/https://doi.org/10.1002/2014JB011547).
- 801 Weaver, A. J., O. A. Saenko, P. U. Clark, and J. X. Mitrovica, 2003: Meltwater pulse 1A from
802 Antarctica as a trigger of the Bølling-Allerød warm interval. *Science*, **299** (5613), 1709–1713,
803 <https://doi.org/10.1126/science.1081002>.
- 804 Zhang, J., 2007: Increasing Antarctic sea ice under warming atmospheric and oceanic conditions.
805 *Journal of Climate*, **20** (11), 2515–2529, <https://doi.org/10.1175/JCLI4136.1>.
- 806 Zhang, J., and D. Rothrock, 2000: Modeling Arctic sea ice with an efficient plastic solution.
807 *Journal of Geophysical Research: Oceans*, **105** (C2), 3325–3338, [https://doi.org/https://doi.
808 org/10.1029/1999JC900320](https://doi.org/https://doi.org/10.1029/1999JC900320).